



**HAL**  
open science

## Metabolomics and lipidomics reveal the effects of the toxic dinoflagellate *Alexandrium catenella* on immune cells of the blue mussel, *Mytilus edulis*

Stéphane Beauclercq, Olivier Grenier, Alexandre Arnold, Dror Warschawski, Gary Wikfors, Bertrand Genard, Réjean Tremblay, Isabelle Marcotte

### ► To cite this version:

Stéphane Beauclercq, Olivier Grenier, Alexandre Arnold, Dror Warschawski, Gary Wikfors, et al.. Metabolomics and lipidomics reveal the effects of the toxic dinoflagellate *Alexandrium catenella* on immune cells of the blue mussel, *Mytilus edulis*. *Harmful Algae*, 2023, 129, pp.102529. 10.1016/j.hal.2023.102529 . hal-04268231

**HAL Id: hal-04268231**

**<https://hal.science/hal-04268231>**

Submitted on 2 Nov 2023

**HAL** is a multi-disciplinary open access archive for the deposit and dissemination of scientific research documents, whether they are published or not. The documents may come from teaching and research institutions in France or abroad, or from public or private research centers.

L'archive ouverte pluridisciplinaire **HAL**, est destinée au dépôt et à la diffusion de documents scientifiques de niveau recherche, publiés ou non, émanant des établissements d'enseignement et de recherche français ou étrangers, des laboratoires publics ou privés.

1 **Metabolomics and lipidomics reveal the effects of the**  
2 **toxic dinoflagellate *Alexandrium catenella* on immune**  
3 **cells of the blue mussel, *Mytilus edulis***

4 Stéphane Beauclercq<sup>a</sup>, Olivier Grenier<sup>b</sup>, Alexandre A. Arnold<sup>a</sup>, Dror E.  
5 Warschawski<sup>c</sup>, Gary H. Wikfors<sup>d</sup>, Bertrand Genard<sup>b,e</sup>, Réjean Tremblay<sup>b\*</sup>,  
6 Isabelle Marcotte<sup>a,\*</sup>

7

8 <sup>a</sup>Department of Chemistry, Université du Québec à Montréal, P.O. Box  
9 8888, Downtown Station, Montréal, QC, Canada

10 <sup>b</sup>Institut des Sciences de la Mer de Rimouski, Université du Québec à  
11 Rimouski, Rimouski, QC, Canada

12 <sup>c</sup>Laboratoire des Biomolécules, LBM, CNRS UMR 7203, Sorbonne  
13 Université, École Normale Supérieure, PSL University, Paris, France

14 <sup>d</sup>Northeast Fisheries Science Center (NEFSC), NOAA Fisheries, Milford, CT,  
15 USA

16 <sup>e</sup>Les laboratoires Iso-BioKem Inc., 367 rue Gratien-Gélinas, Rimouski, QC,  
17 Canada.

18 Corresponding authors: Isabelle Marcotte (marcotte.isabelle@uqam.ca)  
19 and Réjean Tremblay (rejean.tremblay@uqar.ca)

20

21

**22 Abstract**

23 The increasing occurrence of harmful algal blooms, mostly of the  
24 dinoflagellate *Alexandrium catenella* in Canada, profoundly disrupts  
25 mussel aquaculture. These filter-feeding shellfish feed on *A. catenella* and  
26 accumulate paralytic shellfish toxins, such as saxitoxin, in tissues, making  
27 them unsafe for human consumption. Algal toxins also have detrimental  
28 effects upon several physiological functions in mussels, but particularly on  
29 the activity of hemocytes – the mussel immune cells. The objective of this  
30 work was to determine the effects of experimental exposure to *A.*  
31 *catenella* upon hemocyte metabolism and activity in the blue mussel,  
32 *Mytilus edulis*. To do so, mussels were exposed to cultures of the toxic  
33 dinoflagellate *A. catenella* for 120 hours. The resulting mussel saxitoxin  
34 load had measurable effects upon survival of hemocytes and induced a  
35 stress response measured as increased ROS production. The neutral lipid  
36 fraction of mussel hemocytes decreased two-fold, suggesting a differential  
37 use of lipids. Metabolomic <sup>1</sup>H nuclear magnetic resonance (NMR) analysis  
38 showed that *A. catenella* modified the energy metabolism of hemocytes  
39 as well as hemocyte osmolyte composition. The modified energy  
40 metabolism was reinforced by contrasting plasma metabolomes between  
41 control and exposed mussels, suggesting that the blue mussel may  
42 reduce feed assimilation when exposed to *A. catenella*.

43

44

45

46 **Keywords**

47 Paralytic Shellfish Poisoning ; Harmful Algal Bloom ; Mussel immune cells ;

48 Activity assays ; NMR-based metabolomics ; Lipid composition

## 49 1. INTRODUCTION

50 Aquaculture production is increasing worldwide in response to strong  
51 demand for seafood coupled with flat wild fishery landings (FAO, 2020).  
52 The blue mussel, including two species *Mytilus edulis* and *Mytilus*  
53 *trossulus* (Tremblay and Landry, 2016), is an important source of income for  
54 Canadian aquaculture as its production volume and value are the largest  
55 of all harvested molluscs (Statistics-Canada, 2019). Mussel farming occurs in  
56 the natural environment, thus exposing mussels to various environmental  
57 risks, including the presence of toxin-producing microalgae or other  
58 bioactive compounds during harmful algal blooms (HAB) (Lassudrie et al.,  
59 2020), that are expected to increase with climate change (Boivin-Rioux et  
60 al., 2021). As filter-feeding organisms, mussels ingest, assimilate, and  
61 accumulate HAB toxins in their tissues (Galimany et al., 2008a). These  
62 toxins can be harmful to mussels by disrupting several physiological  
63 functions, such as feeding activity, sodium-channel mutation, and valve  
64 microclosures, in some cases leading to tissue damage, paralysis, altered  
65 behavior, and loss of homeostasis (Lavaud et al., 2021; Bianchi et al., 2019;  
66 Comeau et al., 2019; Pousse et al., 2019; Tran et al., 2010; Hegaret et al., 2007;  
67 Bricelj et al., 2005). Microalgal biotoxins can also affect specific cellular  
68 immune-function activities, such as the apoptosis of immune cells or  
69 changes in hematology (Galimany et al., 2008a; Hegaret et al., 2007).

70 The dinoflagellate *Alexandrium catenella*, is recognized as one of the  
71 main, recurring HAB species in Canada (Boivin-Rioux et al., 2021; Starr et al.,  
72 2017; John et al., 2014; Blasco et al., 2003). Dinoflagellate species

73 responsible for HAB produce a complex mixture of toxins from the family  
74 of paralytic shellfish toxins (PSTs), including saxitoxin (STX), neosaxitoxin  
75 (nSTX), gonyautoxin (GTX) and other variants of these molecules (Cusick  
76 and Sayler, 2013).

77 Saxitoxin is recognized as a threat to human health when ingested,  
78 resulting in potentially fatal illnesses (Wang et al., 2003). The toxicity limit  
79 of STX for safe human consumption of bivalve shellfish is 80  $\mu\text{g}$  equivalent  
80 of STX per 100 g of tissue. Distribution and sale of the blue mussel is  
81 forbidden above this threshold (Bates et al., 2020). Previous cultures of *A.*  
82 *catenella* produced at the UQAR aquaculture research station reached  
83 toxin cell quotas ranging between 3 and 60  $\text{pg STX}_{\text{eq}}\cdot\text{cell}^{-1}$  (Lavaud et al.,  
84 2021). Among the bivalve responses to HAB toxins, those in hemocytes,  
85 responsible for innate-immune defense, are the consequence of both the  
86 mechanism of HAB effect and the protective response of the mussels.  
87 Several studies have revealed biotoxins effects on specific cellular  
88 immune-function activities, such as apoptosis of immune cells or changes  
89 in hematology (Galimany et al., 2008b).

90 Hemocytes are specialized bivalve cells involved in digestion,  
91 nutrient transport, excretion, detoxification, shell mineralization, tissue  
92 repair, and, most importantly, immunity (Gosling, 2008). The immune  
93 system of bivalves is exclusively innate and relies upon the circulating  
94 hemocytes to act by phagocytosis or encapsulation of infective agents,  
95 and subsequent elimination of bacteria, cell debris, protozoa, and  
96 potential toxic algae (Cheng, 1996). Blue mussels have been classified as

97 rapid detoxifiers, eliminating toxins within weeks (Lavaud et al., 2021;  
98 Nielsen et al., 2016). PSTs at low doses increase the phagocytic activity of  
99 hemocytes in mussels, with a moderate incidence of lysosomal damage  
100 (Bianchi et al., 2021). This phagocytic activity is thought to modify the  
101 hemocyte lipidome and membrane organization (Leroux et al., 2022).  
102 Hemocyte membrane changes may affect the immune response of  
103 mussels, because the cell membrane is an important participant in  
104 hemocyte immune responses. Specifically, arachidonic acid (20:4n6)  
105 seems to be vital to maintain cellular activities (le Grand et al., 2011, 2013,  
106 2014; Delaporte et al., 2006), but can be targeted by the production of  
107 reactive oxygen species (ROS), another defense mechanism active in  
108 hemocytes (Winston et al., 1996) and arising from mitochondria (Donaghy et  
109 al., 2012). ROS contain one or more unpaired electrons that have high  
110 oxidizing power and rapidly react with compounds having pairs of  
111 electrons, such as double bonds in mono- or poly-unsaturated fatty acids  
112 (MUFA and PUFA) (Turrens, 2003).

113 Knowledge of the biochemical pathways in mussel immune cells  
114 during HAB exposure is limited. Biochemical studies of immune response  
115 to foreign bodies have mostly focused on the hemolymph, the circulatory  
116 fluid of bivalves distributing throughout the body containing nutrients,  
117 respiratory gases, enzymes, metabolic wastes, and toxicants, as well as  
118 hemocytes (Frizzo et al., 2021; Campos et al., 2015). The central role of  
119 hemocytes in the immune system makes them ideal to detect biochemical  
120 responses of mollusks to HAB or other particles; therefore, we

121 investigated the effect of a conspecific HAB upon mussel immune cells  
122 though the application of metabolomics to the hemocytes.

123       Metabolomics provides high-throughput qualitative and quantitative  
124 analyses of metabolites within cells, tissues, or biofluids. Techniques  
125 based upon mass spectrometry (MS) or nuclear magnetic resonance  
126 spectroscopy (NMR) data have been used extensively in biomedical  
127 science, and more recently in the fields of aquaculture and marine  
128 ecology (Bayona et al., 2022; Nguyen and Alfaro, 2020; Young and Alfaro,  
129 2018). Most of these studies have been conducted using MS, and fewer  
130 studies were conducted by NMR spectroscopy, despite its ease of  
131 implementation (Frizzo et al., 2021; Digilio et al., 2016). Proton ( $^1\text{H}$ ) NMR-  
132 based metabolomics was chosen to characterize any biochemical changes  
133 in *M. edulis* hemocytes exposed to *A. catenella*. Furthermore, hemocyte  
134 membrane lipid composition was investigated for its importance in the  
135 phagocytic process. Finally, the effects of a HAB upon *M. edulis* general  
136 metabolism were characterized through NMR analysis of the plasma  
137 separated from the hemocytes. To the best of our knowledge, this study is  
138 the first to apply metabolomics profiling to bivalve hemocytes.

## 139 2. MATERIALS AND METHODS

### 140 2.1 Experimental mussel collection

141       *Mytilus edulis* mussels [length 57.8 (3.7) mm] were sampled in two  
142 batches of 120 individuals each, from aquaculture farm long lines in  
143 Malpeque Bay (Prince Edward Island, Canada, 46.54024N, -63.80926W),  
144 and transported to the wet laboratory research facilities of the Université



145 du Québec à Rimouski (Pointe-au-Père, QC, Canada). Mussels were  
146 scrubbed, rinsed with UV-treated, filtered (1  $\mu\text{m}$ ) seawater and acclimated  
147 for 30 days in two 100 L open-flow tanks with a gradual increase in  
148 temperature for the first 10 days of  $\sim 1^\circ\text{C}$  per day until reaching  $20^\circ\text{C}$ .  
149 During this period, mussels were fed a diet composed of mass-cultured  
150 *Tetraselmis suecica* CCMP 904, *Tisochrysis lutea* CCMP 1324, *Chaetoceros*  
151 *muelleri*, CCMP 1316, and *Diacronema lutheri* CCMP 1325 (1:1:1) at a rate  
152 of  $4 \times 10^7$  cells·indiv<sup>-1</sup>·day<sup>-1</sup> (equivalent to 1% of dry weight per day). Algal  
153 strains were obtained from the Provasoli-Guillard National Center for  
154 Marine Algae and Microbiota (NCMA, Maine, USA) and cultured in  
155 autoclaved 20 L bottles with F/2-Si nutrient enrichment, daylight 24/0  
156 (D/N) at light intensity of  $100 \mu\text{m} \cdot \text{m}^{-2} \cdot \text{s}^{-1}$  PAR at  $20^\circ\text{C}$ .

157 An *Alexandrium catenella* isolate (clone named AC6, Lavaud et al. 2021)  
158 was obtained from the St. Lawrence Estuary (Canada) during a bloom  
159 monitored in 2008 (Starr et al., 2017) and grown under the same axenic  
160 conditions as the non-toxic microalgae, generating toxin cell quotas  
161 between 3 and 60 pg STXeq·cell<sup>-1</sup> (Lavaud et al., 2021).

## 162 **2.2 Exposure of mussels to cultured *Alexandrium catenella***

163 Mussels from each batch were brushed with diluted hypochloric acid  
164 (<1%), rinsed with UV-treated, filtered (1  $\mu\text{m}$ ) seawater, and distributed  
165 into eight 30 L conical-bottom tanks (15 mussels per tank) filled with UV-  
166 treated, 0.1  $\mu\text{m}$ -filtered seawater at  $20^\circ\text{C}$  with food addition similar to that  
167 of the acclimation period. A volume representing 50% of the seawater in  
168 each tank was changed daily. During the 120 h of the experiment,

169 mussels in four tanks were fed *A. catenella* daily by peristaltic pumps at a  
170 concentration of  $182 \text{ cells}\cdot\text{mL}^{-1}$  (equivalent to  $3.6\times 10^5 \text{ cells}\cdot\text{ind}^{-1}\text{d}^{-1}$  or 1%  
171 of their dry weight) in addition to the acclimation diet. In the control  
172 treatment, mussels in four other tanks were supplemented with  $520$   
173  $\text{cells}\cdot\text{mL}^{-1}$  per day of cultured *Tetraselmis suecica* (in addition to the  
174 acclimation diet), to obtain similar microalgal biomass in both treatments.  
175 During the experimental period, no mussel mortality or spawning event  
176 was observed.

### 177 **2.3 Hemocyte sampling**

178 After 120 h of exposure to toxic algae, mussels were sampled in each  
179 tank. The hemolymph (0.5 to 1 mL) was collected from the pericardial  
180 cavity/adductor muscle sinus with a sterile, 21G gauge needle using a 1  
181 mL syringe. Hemolymph samples were filtered through an  $80 \mu\text{m}$  mesh  
182 and stored in Eppendorf microcentrifuge tubes held on ice, for cell activity  
183 analyses and hemocyte morphology of individual mussels with the first  
184 batch, and for solution NMR-based metabolomics with the second batch.  
185 No intermediate sampling of hemolymph was performed to be able to collect  
186 enough hemocyte for the NMR measurements after the 120 h of exposure  
187 to *A. catenella*.

188 For solution NMR analysis, the hemolymph was combined into six pools  
189 from 10 mussels randomly collected among the 60 mussels in the four  
190 tanks for each treatment, in 15 mL conical-bottom centrifuge tubes kept  
191 on ice, and immediately centrifuged at  $800\times g$  at  $4^\circ\text{C}$  for 15 min to  
192 separate the hemocytes from the plasma (Frizzo et al., 2021). Hemocyte

193 recovery was 100 to 200 mg from the hemolymph in each pool. The  
194 pelleted hemocytes and plasma fractions were transferred into new 15  
195 mL, conical-bottom centrifuge tubes and frozen immediately at  $-80^{\circ}\text{C}$   
196 until metabolite extraction.

197 For lipid composition analysis of the first batch, the remaining  
198 hemolymph and hemocytes were randomly pooled together into three  
199 samples (20 mussels/sample) per treatment, centrifuged ( $8,000\times g$ , for 5  
200 min at  $4^{\circ}\text{C}$ ), and the supernatant was partially removed. The hemocytes  
201 were rinsed 5 times with  $0.2\ \mu\text{m}$ -filtered seawater and centrifuged under  
202 the same conditions for 2 min. The 6 samples of purified hemocytes were  
203 then placed in 2 mL amber glass vials with Teflon-lined caps.

#### 204 **2.4 Cell activity analyses**

205 Procedures for characterization of the hemocytes, granular/agranular  
206 subpopulations, hemocyte mortality, state of apoptosis of dead or living  
207 cells, percentage of apoptotic cells, and unstimulated hemocyte  
208 production of ROS were adapted from previous studies (Donaghy et al.,  
209 2012; Galimany et al., 2008b; Soudant et al., 2004; Hegaret et al., 2003). The  
210 hemocytes and plasmas were extracted from the six pools of hemolymph  
211 for each treatment, as described above. Hemocyte counting was carried  
212 out using a BD Accuri™ C6 flow cytometer (BD Biosciences, San Jose, CA,  
213 USA). The detection method used for the hemocytes involved staining one  
214 subsample with SYBR Green (a DNA-binding probe which spontaneously  
215 penetrates both viable and dead cells) to detect all hemocytes, and  
216 propidium iodide (PI) to detect dead cells. To differentiate cells

217 undergoing apoptosis, another subsample was stained with both PI and  
218 AnnexinV, which is a membrane inversion marker, an early step in  
219 programmed cell death (PCD). This method allows the detection of four  
220 cell types in a single assay: non-apoptotic living cells, apoptotic living cells  
221 (the membrane has inverted as an early step in PCD but the membrane  
222 remains impermeable to PI), apoptotic dead cells (permeable to PI and  
223 membrane has inverted), and non-apoptotic dead cells (permeable to PI  
224 and membrane has not inverted, cells have died by necrosis).

225 *M. edulis* hemocytes are composed of two subpopulations,  
226 agranulocytes and granulocytes, whose morphology was determined  
227 based upon flow-cytometric parameters, Forward Scatter (FSC) and Side  
228 Scatter (SSC), as described in Donaghy et al. (2012). FSC and SSC  
229 commonly measure particle size and internal complexity in arbitrary units  
230 (AU), respectively.

231 Determination of ROS production was performed using 2',7'-  
232 dichlorofluorescein diacetate (DCFH-DA; Molecular Probes, Invitrogen), at  
233 a final concentration of 10  $\mu$ M, a membrane permeable and non-  
234 fluorescent probe as described in Donaghy et al. (2012). Inside  
235 hemocytes, the -DA radical is hydrolyzed by esterase enzymes. DCFH is  
236 oxidized by intracellular hydrogen peroxide ( $H_2O_2$ ) and superoxide ion to  
237 the fluorescent DCF molecule. DCF green fluorescence was detected on  
238 the FL1 detector (530/30 nm band pass) of the flow cytometer, and it is  
239 proportional to cellular ROS production. Relative ROS production is  
240 expressed as DCF fluorescence in arbitrary units (FAU).

## 241 **2.5 Lipid composition**

242 Hemocytes were pooled into three samples per treatment, as described  
243 above, and lipids were extracted by grinding the hemocyte samples in  
244 dichloromethane-methanol using a modified Folch procedure as described  
245 in Parrish (1999). The lipid content and class composition were determined  
246 using a flame-ionization detection system (Parrish, 1987), with silica-gel-  
247 coated chromarods (S-V Chromarods; Shell-USA). Each lipid extract was  
248 scanned by an Iatroscan (Mark-VI, Iatron Laboratories) to separate  
249 aliphatic wax esters, ketones, triacylglycerols, alcohols, sterols, acetone  
250 mobile polar lipids, and phospholipids. For each lipid class, standards were  
251 used (Sigma Aldrich, Oakville, Canada). Chromatograms were analyzed  
252 using the integration software Peak Simple version 3.2 (SRI). Total lipids  
253 (expressed as  $\mu\text{g}\cdot\text{mg}^{-1}$ ) are the sum of all classes, and each class is  
254 expressed as relative concentration (% of total lipids).

255 Lipid extracts were separated into neutral and polar fractions by column  
256 chromatography on silica-gel micro-columns (30×5 mm i.d., packed with  
257 Kieselgel 60, 70–230  $\mu\text{m}$  mesh; Merck, Darmstadt, Germany) using  
258 chloroform:methanol (98:2, v/v) to elute neutral lipids, followed by  
259 methanol to elute polar lipids (Marty et al., 1992). Fatty-acid profiles of  
260 polar lipids were determined on fatty-acid methyl esters (FAMES) using  
261 sulfuric acid:methanol (2:98, v:v) and toluene. FAMES of neutral and polar  
262 fractions were concentrated in hexane, and the neutral fraction was  
263 purified on an activated silica gel with 1 mL of hexane:ethyl acetate (v/v)  
264 to eliminate free sterols. FAMES were analysed in the full scan mode (ionic

265 range: 50–650 m/z) on a Polaris Q ion-trap-coupled multichannel gas  
266 chromatograph “Trace GC ultra” (Thermo Scientific, MA, USA) equipped  
267 with an autosampler model Triplus, a PTV injector, and a mass detector  
268 model ITQ900 (Thermo Scientific, MA, USA). The separation was  
269 performed with an Omegawax 250 (Supelco) capillary column with high  
270 purity helium as the carrier gas. Data were treated using Xcalibur v.2.1  
271 software (Thermo Scientific, MA, USA). Tricosanoic acid (23:0) was  
272 employed as an internal standard. FAMES were identified and quantified  
273 using known standards (Supelco 37 Component FAME Mix and menhaden  
274 oil; Supelco), and were further confirmed by MS.

## 275 **2.6 Hemocyte and plasma extraction for solution NMR**

276 Metabolites were extracted from the 6 pools of hemocytes from 10  
277 mussels per treatment, using an adaptation of Folch’s method (Madji  
278 Hounoum et al., 2015). Briefly, 3 mL of ice-cold methanol followed by 3 mL  
279 of dichloromethane were added to the conical centrifuge tubes containing  
280 the hemocytes previously thawed on ice. The mixtures were vortexed for  
281 1 min and sonicated (Cole-Parmer Ultrasonic cleaner 08892, Vernon Hills,  
282 IL, USA) on ice for 10 min before addition of 2 mL cold, extra-pure water  
283 and 30 s agitation. Following cooling at –20°C for 40 min to precipitate  
284 proteins, the samples were centrifuged at 7,100×g at 4°C for 15 min to  
285 separate the polar and lipidic fractions. The polar fractions were collected  
286 in glass tubes, and the solvent was evaporated in a SpeedVac (Thermo  
287 Fisher Scientific, Waltham, MA, USA) at room temperature. Plasma  
288 samples for <sup>1</sup>H NMR were prepared by cold methanol precipitation of lipids

289 and proteins (Beauclercq et al., 2016). Briefly, 500  $\mu$ L of unfrozen plasma  
290 samples were mixed with 1 mL of ice-cold methanol and cooled at  $-20^{\circ}\text{C}$   
291 for 20 min. The mixes were then centrifuged at  $15,000\times g$  at  $4^{\circ}\text{C}$  for 10  
292 min, and the supernatants were collected in microtubes for further solvent  
293 evaporation in a SpeedVac at room temperature.

## 294 **2.7 Solution NMR-based metabolomics**

### 295 **2.7.1 NMR spectroscopy measurements**

296 Prior to NMR analysis, hemocyte extracts and plasma samples were  
297 reconstituted in 500  $\mu$ L of 0.2 M pH 7.4 potassium phosphate buffer in  
298 99.9% deuterium oxide ( $\text{D}_2\text{O}$ ) with 0.13 mM 3-trimethylsilylpropionic acid  
299 (TSP) as the internal standard. Mixtures were briefly vortexed and  
300 centrifuged at  $2,000\times g$  for 30 s to remove insoluble components. The  
301 resulting supernatants were transferred to 5 mm NMR tubes for analysis.

302 The  $^1\text{H}$  NMR spectra from the hemocyte extracts and plasma samples  
303 were obtained with a Bruker Avance III spectrometer (Billerica, MA, USA),  
304 operating at 600 MHz, with a broad-band inverse TXI probe. NMR  
305 measurements were performed at 298 K. The spectra were acquired using  
306 a 1D NOESY pulse sequence with a repetition delay of 10 s and mixing  
307 time of 50 ms. Water suppression was achieved by presaturation during  
308 the repetition delay and mixing time.  $^1\text{H}$  spectra were collected with 1,024  
309 or 256 scans (and eight dummy scans) for the hemocyte extracts or  
310 plasma, respectively, in 64k data points with a spectral width of 12 ppm.  
311 Spectral data were deposited under the DOI 10.5281/zenodo.7415126 in

312 the Zenodo repository (<https://zenodo.org>) hosted by the European  
313 Organization for Nuclear Research (CERN).

### 314 **2.7.2 NMR spectra post-processing**

315 Spectra were processed using NMRProcFlow tools (Jacob et al., 2017).  
316 The free induction decays (FIDs) were zero-filled to 128k data points, a  
317 line-broadening factor of 0.3 Hz was applied prior to Fourier  
318 transformation, and the TSP reference signal was set to 0 ppm. NMR  
319 spectra were further processed for peak alignment with NMRProcFlow to  
320 minimize spectral peak shift caused by differences in ionic strength within  
321 samples. The hemocyte extracts and plasma spectra were then bucketed  
322 manually and integrated into 97 and 138 spectral regions (corresponding  
323 to one or several metabolites), respectively. The signals from water and  
324 methanol were excluded, and the data were normalized by the total sum  
325 of all the spectral features, which assumes that only small amounts of  
326 metabolites are regulated in approximately equal shares up and down,  
327 while all others remain constant (Zacharias et al., 2018). The generated  
328 data tables for the hemocyte extracts and plasma were used for  
329 multivariate statistical analyses.

### 330 **2.7.3 Spectral assignment**

331 The identification of metabolites was performed using Chenomx  
332 software (Edmonton, Canada), HMDB <https://hmdb.ca/> (Wishart et al.,  
333 2022), and reference publications on mollusc NMR-based metabolomics  
334 (Frizzo et al., 2021; Aru et al., 2020). The annotations of the spectra were  
335 further confirmed by 2D  $^1\text{H}$  NMR COSY and TOCSY experiments performed



336 on a representative sample. The acquisition parameters for those two  
337 experiments are provided in Table S1.

## 338 **2.8 Mussel weight, volume and toxin concentration**

339 At the end of the experiments, soft tissues of each mussel were  
340 individually lyophilized to measure the dry mass and estimate the  
341 condition index (CI, in  $\text{g}/\text{mm}^3$ ) as the ratio of tissue dry weight ( $\text{DW}_{\text{tissue}}$ ,  
342 g) over volume ( $V$ ,  $\text{mm}^3$ ). The latter was estimated from the measurement  
343 of shell length, width and height with a digital caliper (Mitutoyo 500-196-  
344 30 AOS absolute; precision of 0.01 mm). As all the blood was used for flow  
345 cytometry and NMR measurement, the amount of saxitoxin was estimated  
346 in the whole tissue of each mussel by MS, using a Triple Quad (6420  
347 Agilent Technologies) and Poroshell 120 column (HILIC-Z, 2.1x100 mm, 3  
348  $\mu\text{m}$ ), with a certified standard from the National Research Council Canada  
349 (NRC CRM-STX-g, MRC, Halifax, Ca). The saxitoxin dosage protocol is  
350 detailed in the supplementary file.

## 351 **2.9 Statistical analyses**

352 Values for each hemocyte characteristic and mussel condition index for  
353 exposed and non-exposed (control) mussels were compared by Student's  
354 *t*-test, following validation of normality and homoscedasticity using the  
355 Shapiro-Wilk test. Additionally, linear regression analyses were used  
356 between each hemocyte characteristics and saxitoxin concentration in  
357 mussel tissues to estimate possible relationships between toxins and  
358 hemocyte activities. Standard deviations are indicated in plot brackets.

359 For the lipid composition of hemocytes, as individual samples were  
360 pooled, the replication level corresponded to the tanks (3 for control and 3  
361 for toxic treatment). A distance-based permutational multivariate analysis  
362 of variance (PERMANOVA) was used to compare multivariate variables  
363 (lipid classes and FA profiles) following assumptions of homoscedasticity  
364 verified with the PERMDISP test. *A posteriori* comparisons were done using  
365 a PERMANOVA pairwise test. To analyze the similarity between the  
366 profiles, non-metric, multi-dimensional scaling (nMDS) and SIMPER  
367 analyses were performed, using Euclidian distances. These statistical  
368 analyses were done using PRIMER 7.0.21. The significance of the  
369 difference between groups was further evaluated through Welch's t-test.

370 An orthogonal projection latent structures discriminant analyses (OPLS-  
371 DA) was performed using the Umetrics SIMCA 17 software (Sartorius  
372 Stedim, Göttingen, Germany) on hemocyte extracts and plasma  $^1\text{H}$  NMR  
373 data sets. All data were scaled to units of variance. The minimum number  
374 of features needed for optimal classification of the OPLS-DA models was  
375 determined by iteratively excluding the variables with low regression  
376 coefficients and wide confidence intervals derived from jackknifing  
377 combined with low variable importance in the projection (VIP) until  
378 maximum improvement of the quality of the models (Beauclercq et al.,  
379 2022). The model quality was evaluated after 7-fold cross validation by  
380 cumulative  $R^2Y$  (goodness of fit), cumulative  $Q^2$  (goodness of prediction)  
381 and CV-ANOVA (test of cross-validated predictive residuals to assess the  
382 reliability of OPLS models). The contribution of each predictor in the model  
383 was evaluated through the variable score contribution, i.e., the

384 differences, in scaled units, for all the terms in the model, between the  
385 outlying and the normal observation, multiplied by the absolute value of  
386 the normalized weight.

### 387 3 **RESULTS**

#### 388 **3.1 Mussel condition index and hemocyte count**

389 To monitor the effect on the blue mussels of a 120 h exposure to *A.*  
390 *catenella*, we determined the condition index, *i.e.*, the relationship  
391 between body dry weight and shell length. We also performed a hemocyte  
392 count. First, we measured the soft-tissue concentrations of saxitoxin  
393 following exposure and hemolymph sampling, which ranged from 3 to 95  
394  $\mu\text{g STX}/100\text{ g}$ , with a mean of 26 (22)  $\mu\text{g STX}/100\text{g}$  of mussels. At the end  
395 of the exposure, no significant difference ( $p = 0.08$ ) in condition index was  
396 observed between exposed mussels [13.0 (2.5)  $\text{g}/\text{mm}^3$ ] and the control  
397 [11.6 (2.1)  $\text{g}/\text{mm}^3$ ]. Also, the hemocyte count was similar for the exposed  
398 [2258 (2108)] and control mussels [1727 (866),  $p = 0.25$ ].

#### 399 **3.2 Apoptotic activity and ROS production**

400 We also evaluated hemocyte apoptotic activity and ROS production, by  
401 flow cytometry with four different probes for possible changes associated  
402 with exposure to *A. catenella*. As shown in Table 1, exposure to toxic  
403 dinoflagellates modified hemocyte activity, including four major variables  
404 related to apoptosis. Specifically, when mussels were exposed to *A.*  
405 *catenella*, the percentage of apoptotic dead cells ( $p = 0.009$ ), non-  
406 apoptotic dead cells ( $p = 3.95 \times 10^{-7}$ ) and apoptotic living cells ( $p =$   
407  $1.10 \times 10^{-3}$ ) decreased, but the mean percentage of non-apoptotic living

408 cells was significantly higher ( $p = 2.77 \times 10^{-5}$ ) as compared to the control.  
 409 There were no significant correlations between hemocyte apoptotic-  
 410 associated variables and the saxitoxin concentration measured in the  
 411 whole mussel tissues (Table S2). Thus, regardless of the concentration of  
 412 saxitoxin, most cells remained alive and non-apoptotic in mussels  
 413 exposed to *A. catenella*.

414 **Table 1.** Hemocyte apoptotic status variables determined by flow  
 415 cytometry for control mussels and mussels exposed (120 h) to *A.*  
 416 *catenella*. Variables are presented as [mean (standard deviation)] and  
 417 with statistical t-Tests on the means differences. Differences with  
 418 statistical significance ( $p \leq 0.05$ ) are highlighted with bold characters, and  
 419 the directions of the variations are indicated by arrows.  
 420

	Control	Exposed	t-Test
421 % <b>non-apoptotic living cells</b>	<b>60.99 (14.73)</b>	<b>↑ 84.70 (19.99)</b>	<b><math>2.77 \times 10^{-5}</math></b>
422 % <b>non-apoptotic dead cells</b>	<b>28.95 (11.88)</b>	<b>↓ 10.60 (12.76)</b>	<b><math>3.95 \times 10^{-7}</math></b>
423 % <b>apoptotic living cells</b>	<b>2.40 (2.57)</b>	<b>↓ 0.78 (1.42)</b>	<b><math>1.10 \times 10^{-3}</math></b>
% <b>apoptotic dead cells</b>	<b>7.65 (8.01)</b>	<b>↓ 3.91 (9.1)</b>	<b><math>8.90 \times 10^{-3}</math></b>
424 Agranulocyte complexity (AU)	2.69 (0.14) $\times 10^4$	2.67 (0.23) $\times 10^4$	0.36
425 <b>Granulocyte complexity (AU)</b>	<b>2.94 (0.30) <math>\times 10^5</math></b>	<b>↓ 2.71 (0.45) <math>\times 10^5</math></b>	<b>0.05</b>
426 Size agranulocyte (AU)	6.22 (0.17) $\times 10^5$	6.16 (0.23) $\times 10^5$	0.29
427 Size granulocyte (AU)	2.19 (0.17) $\times 10^6$	2.17 (0.17) $\times 10^6$	0.78
428 % alive agranulocytes	49.07 (13.07)	45.08 (9.46)	0.22
% alive granulocytes	19.41 (6.86)	19.60 (5.11)	0.80
429 % <b>dead agranulocytes</b>	<b>14.37 (2.49)</b>	<b>↑ 16.16 (2.92)</b>	<b>0.04</b>
% dead granulocytes	17.15 (6.23)	19.16 (5.82)	0.24
<b>ROS agranular cells (FAU)</b>	<b>2306 (416)</b>	<b>↑ 3622 (1612)</b>	<b><math>5.27 \times 10^{-6}</math></b>
ROS granular cells (FAU)	73017 (44002)	81618 (52059)	0.19

430 subpopulations of hemocytes differing in size and granularity were  
 431 identified, *i.e.*, the granulocytes and agranulocytes. The granulocytes,

Two

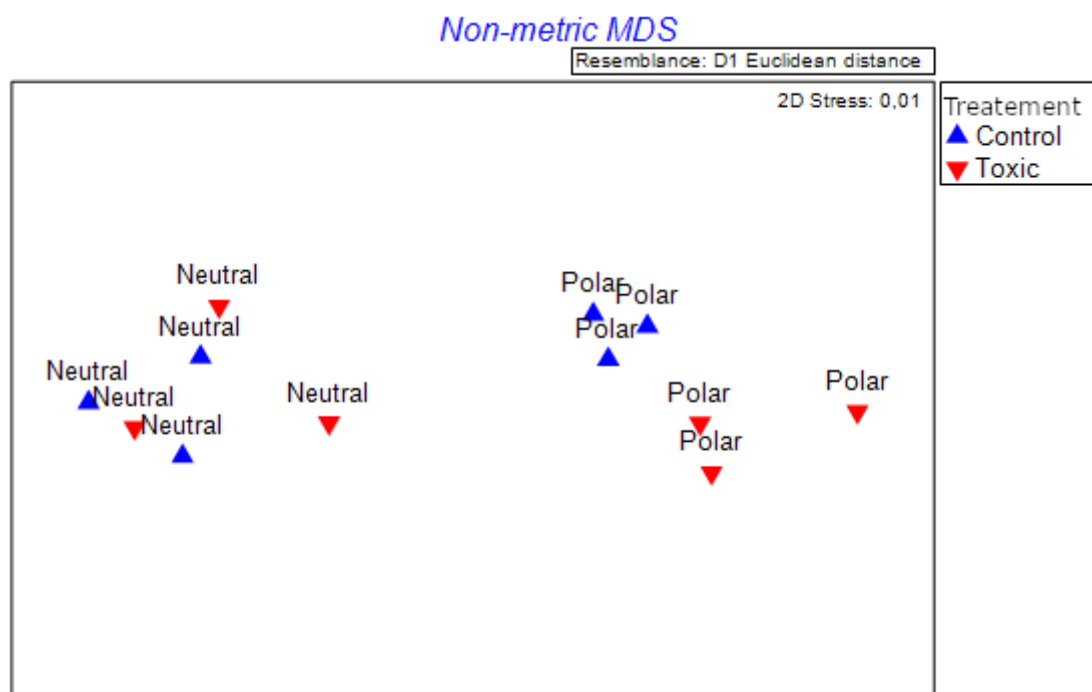
432 which contain granules, were larger than the agranulocytes and  
433 accounted for ~40% of all hemocytes (Table 1). Although the majority of  
434 granulocytes and agranulocytes were alive in both treatments, the  
435 exposure to *A. catenella* induced a higher mortality percentage in the  
436 agranulocyte population ( $p = 0.035$ ) as well as a 1.6-time rise in ROS  
437 production ( $p = 5.27 \times 10^{-6}$ ). Moreover, the complexity, or granularity, of  
438 the granulocytes, was significantly higher in the “toxic” treatment ( $p =$   
439 0.05).

### 440 **3.3 Lipid composition of hemocyte membranes**

441 Lipid composition analysis of the hemocyte membranes revealed  
442 differences between the polar and neutral fractions (DF = 1 and 11,  
443 Pseudo-F = 6249,  $p = 0.0001$ ). Indeed, the polar fraction showed the  
444 presence of 56% phospholipids and the absence of triglycerides; whereas,  
445 the neutral fraction contained 55% triglycerides and no phospholipids.  
446 Simper analysis indicated that these two lipid classes explain more than  
447 83% of the dissimilarity between the polar and neutral lipid profiles. Both  
448 hemocyte lipid fractions had similar lipid class composition, whether  
449 exposed or not to *A. catenella* (Figure 1). Total lipids, however,  
450 represented by the sum of the concentration of each lipid class, showed  
451 significant interactions between lipid fractions (neutral and polar) and  
452 conditions (DF = 1 and 11, Pseudo-F = 13,  $p = 0.0064$ ). Differences  
453 attributable to the toxic exposure were not observed in the polar fraction,  
454 in contrast to the neutral fraction in toxin-exposed mussels, which showed

455 less than half the lipid concentration ( $p = 0.0092$ ) of the control [300 (50)  
 456 vs. 650 (130)  $\text{mg}\cdot\text{g}^{-1}$  dry mass].

457



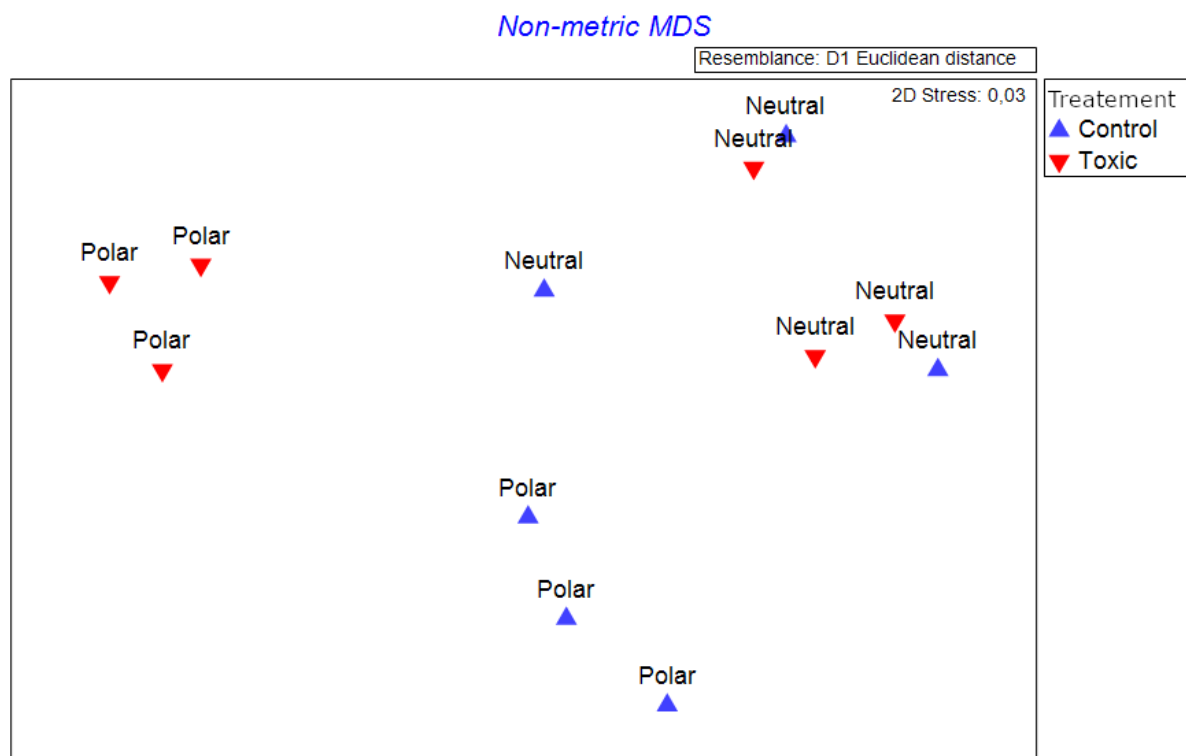
458

459 **Figure 1.** Non-metric multi-dimensional scaling of the Euclidian similarity  
 460 matrix based on the relative abundance of lipids classes in the neutral and  
 461 polar lipid fractions of hemocytes exposed (Toxic, blue) or not (Control,  
 462 red) to *A. catenella*.

463

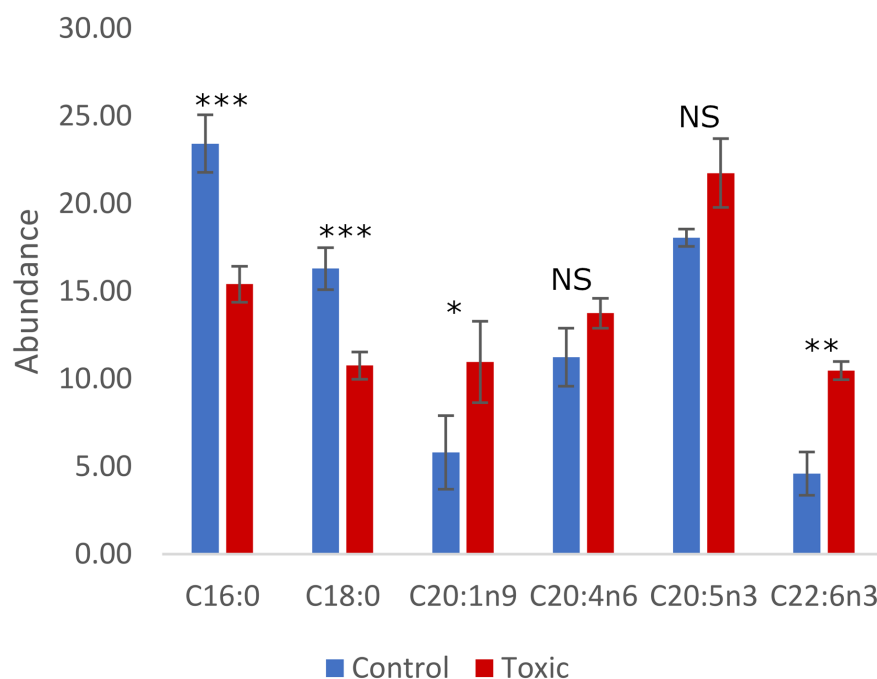
464 The fatty acid (FA) profiles of the lipid fractions from the hemocytes of  
 465 mussels exposed to the PST-producing dinoflagellate and from those  
 466 exposed to the forage *T. suecica* algae were different (Figure 2). A  
 467 significant interaction was observed (DF = 1 and 11, Pseudo-F = 5.25,  $p =$   
 468 0.0108), and associated with differences in the FAs profile only in the  
 469 polar fraction ( $p = 0.0049$ ), but not in the neutral fraction ( $p = 0.8365$ ).  
 470 The Simper analysis indicates that these are related to the saturated FAs  
 471 16:0 (19.3%) and 18:0 (9.4%), with relative abundances higher in the

472 control ( $p = 0.004$ ), as well as the unsaturated FAs 20:5n3 (29.5%),  
 473 20:4n6 (9.7%), 20:1n9 (8.9%), 22:6n3 (8.2%) in higher abundance in the  
 474 toxic group (Figure 3). The differences between groups were significant ( $p$   
 475  $\leq 0.05$ ) for C16:0, C18:0, C20:1n9, and C22:6n3.



477 **Figure 2.** Non-metric multi-dimensional scaling of the Euclidian similarity  
 478 matrix based on the relative abundance of fatty acids in the neutral and  
 479 polar lipid fractions of hemocytes exposed (Toxic, red) or not (Control,  
 480 blue) to *A. catenella*.

481



482

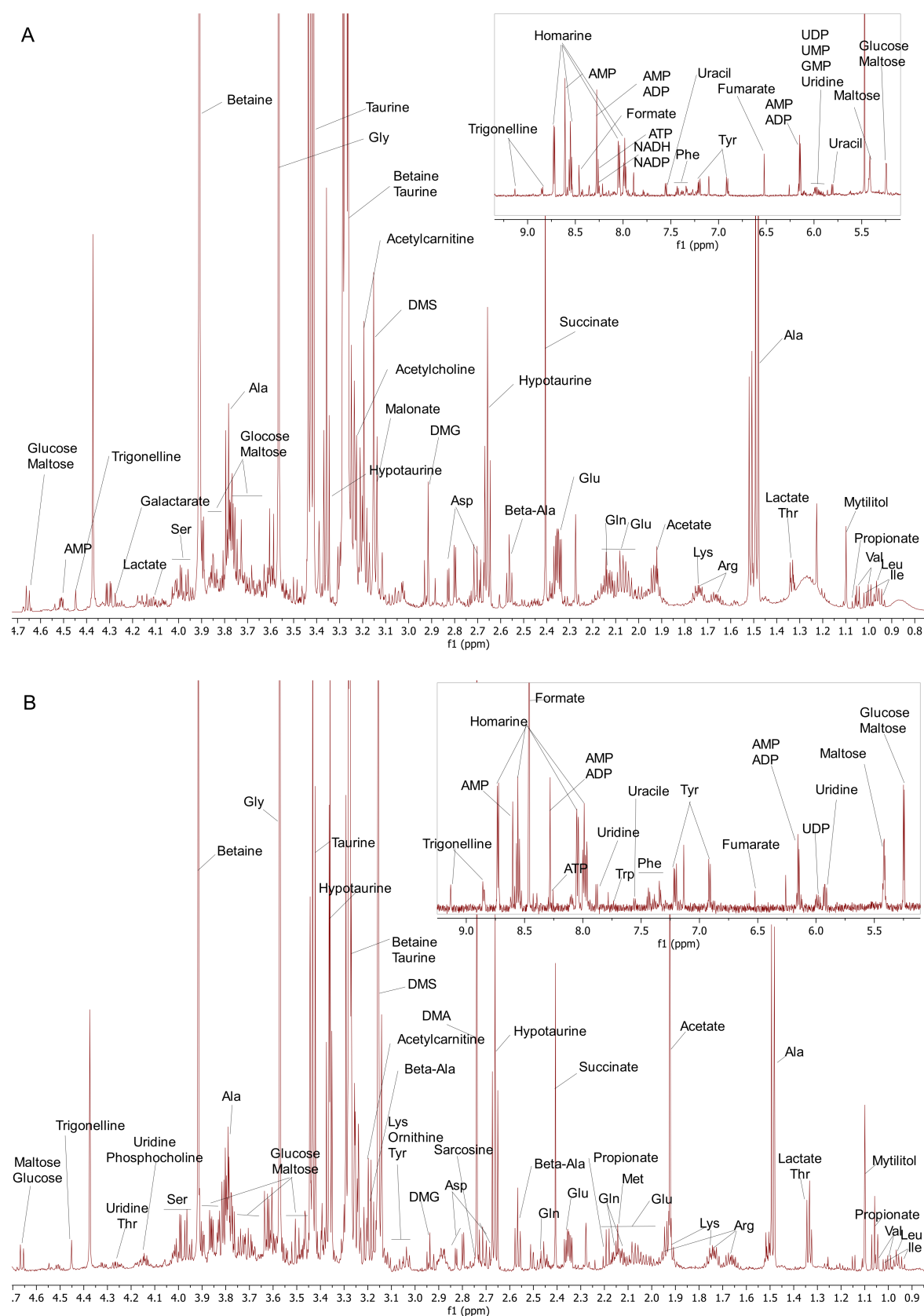
483 **Figure 3.** Relative abundances of the six fatty acids in the polar lipid  
 484 fraction that contributed to 85% of the differences between hemocytes  
 485 exposed (Toxic, red) or not (Control, blue) to *A. catenella* in Simper  
 486 analysis. The significance of the differences between groups was further  
 487 evaluated through Welch's t-test (P-value NS > 0.05, \* ≤ 0.05, \*\* ≤ 0.01,  
 488 \*\*\* ≤ 0.005).

489

### 490 3.4 Hemocyte and plasma metabolomes by solution NMR

491 Annotated representative <sup>1</sup>H NMR spectra of the hemocyte extracts and  
 492 of the plasma are shown in Figure 4. The NMR spectra were divided into  
 493 97 and 138 buckets corresponding to 59 and 55 identified metabolites for  
 494 the hemocyte extracts and the plasma samples, respectively. The  
 495 percentage of unidentified buckets were 17% in the spectra of the  
 496 hemocyte extracts and 15% in the plasma samples. The identified  
 497 metabolites belonged mainly to 5 classes: amino acids, FAs and  
 498 conjugated, purines, pyrimidines, and tricarboxylic acid cycle (TAC) acids.

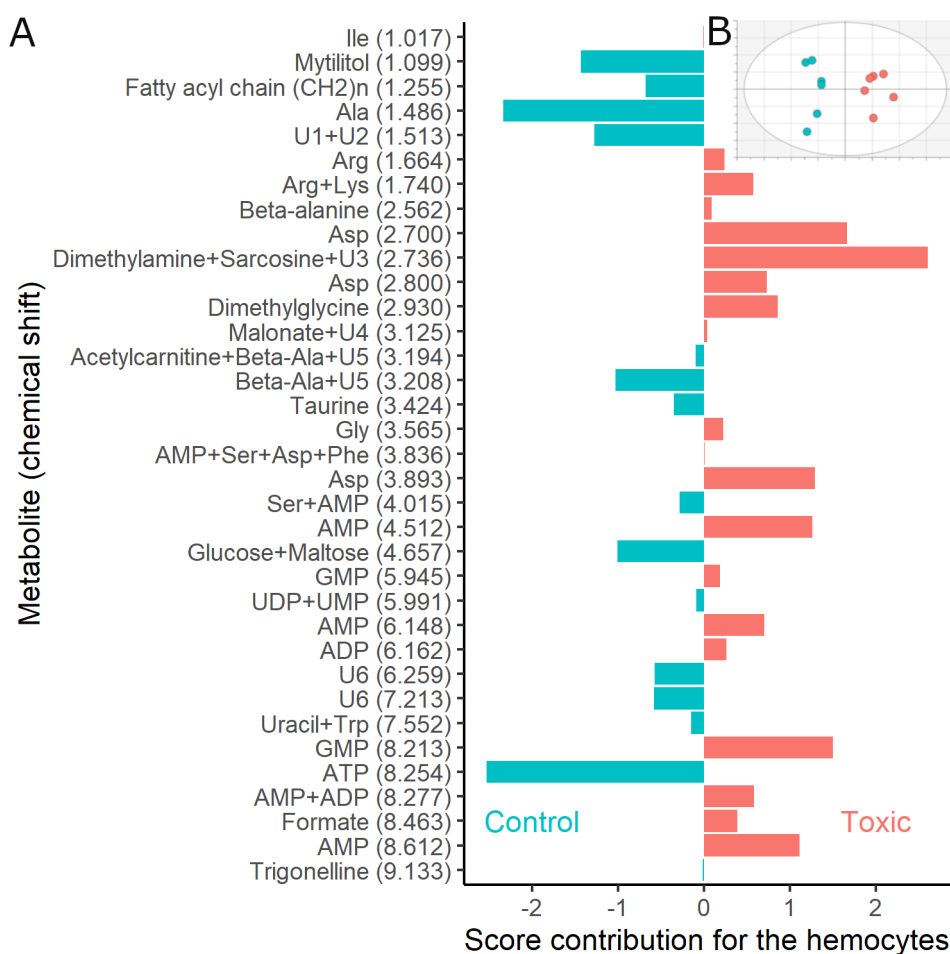




499

500 **Figure 4.** Representative annotated  $^1\text{H}$  NMR spectra of (A) the hemocyte  
 501 extract and (B) plasma. DMA: dimethylamine, DMG: dimethylglycine, DMS:  
 502 dimethyl sulfone.

503 OPLS-DA models were adjusted to the metabolome of the hemocytes  
504 and plasma of mussels exposed or not to *A. catenella* to explore possible  
505 effects of the toxic dinoflagellate upon the immune system and general  
506 metabolism of the mussels. The first model was fitted to the hemocyte  
507 metabolomics data and contained a subset of 35 buckets corresponding  
508 to 28 identified metabolites (Figure 5). The model was composed of one  
509 predictive and one orthogonal component with an explicative ability ( $R^2Y$ )  
510 of 0.94 and a predictive ability ( $Q^2$ ) of 0.71 (CV-ANOVA = 0.05). The  
511 metabolites included in the models belonged mainly to the classes of  
512 amino acids, purines, and pyrimidines. Purines such as adenosine  
513 monophosphate (AMP), adenosine diphosphate (ADP), and guanosine  
514 monophosphate (GMP), amines (dimethylamine), carboxylic acids  
515 (formate), and some amino acids (dimethylglycine, glycine, phenylalanine,  
516 isoleucine, lysine, aspartic acid, sarcosine, arginine) were more plentiful in  
517 the hemocytes after toxic treatment. On the other hand, alanine, serine,  
518 tyrosine and the purine adenosine triphosphate (ATP) as well as  
519 pyrimidines (uridine monophosphate (UMP), uridine diphosphate  
520 UDP/UDP-glucose, uracil), sulfonic acids (taurine), disaccharides (maltose),  
521 alkaloids (trigonelline), monosaccharides (glucose), benzamides  
522 (mytilitol), and fatty esters (acetylcarnitine) were lower in the hemocyte  
523 extracts of mussels exposed to the toxic treatment.

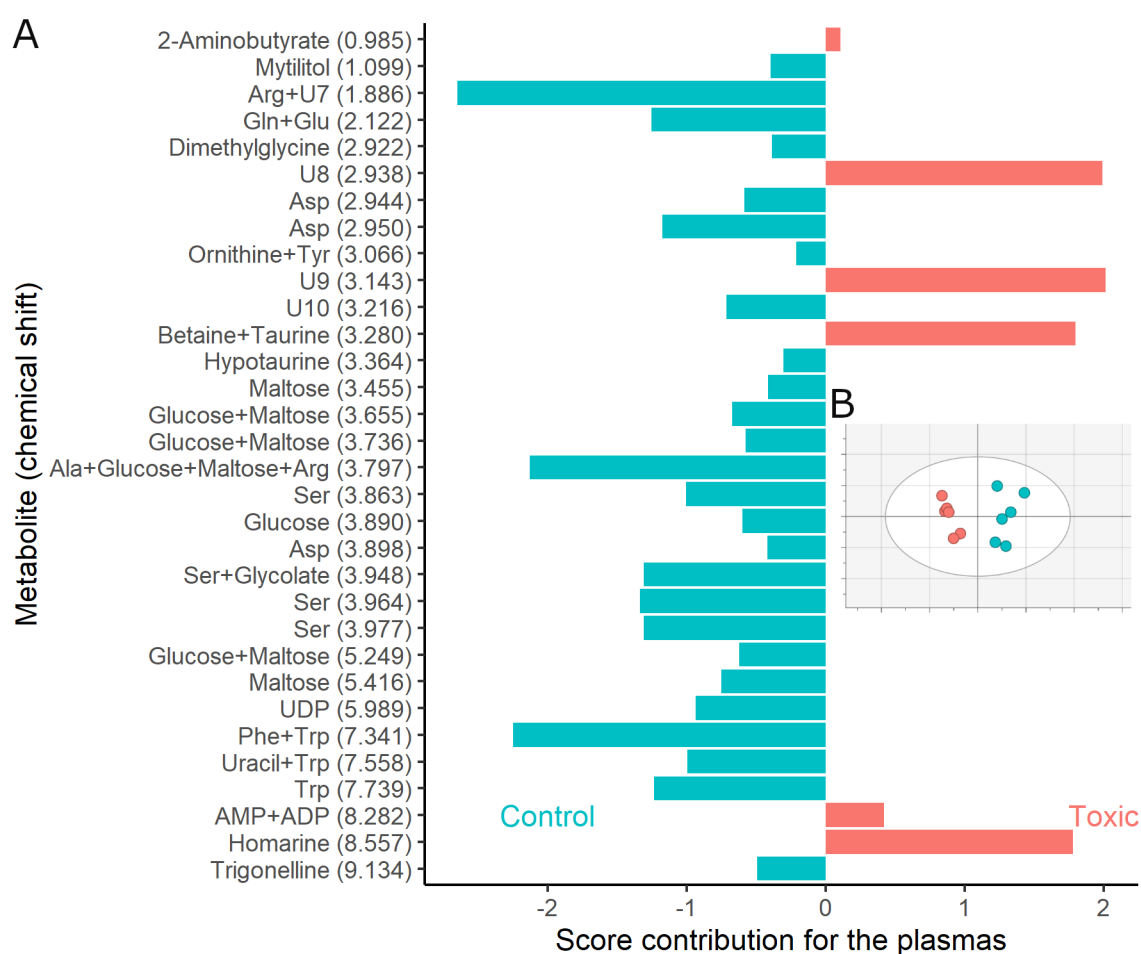


524

525 **Figure 5.** Metabolomic analysis of the effect on the hemocytes of a 120h  
 526 exposure to *A. catenella*. (A) Contributions plot, indicative of the  
 527 contribution of hemocyte metabolites identified in the OPLS-DA. (B) Score  
 528 plots following OPLS-DA with the treatment as categorical factor Y and the  
 529 metabolites as explanatory qualitative variables X. The hemocyte samples  
 530 exposed to *A. catenella* and the control are represented by pink and  
 531 turquoise circles, respectively. The model contained 35 buckets, 1  
 532 predictive and 1 orthogonal components, and its descriptive and  
 533 predictive performance were  $R^2Y = 0.94$  and  $Q^2 = 0.71$ .

534 The second OPLS-DA model based on plasma data aimed to assess the  
 535 effects of an exposure to *A. catenella* on the global metabolism of the  
 536 mussels (Figure 6). This model was composed of 32 buckets projected to  
 537 one predictive and one orthogonal components with a  $R^2Y$  of 0.92 and a  $Q^2$   
 538 of 0.78 (CV-ANOVA = 0.02). As for the hemocytes, the 25 metabolites in  
 539 the model were mostly amino acids, purines, and pyrimidines. Amino  
 540 acids (dimethylglycine, Glu, Tyr, Phe, Ala, Ser, Asp, Ornithine, Arg, Gln,

541 Trp), pyrimidines (UDP, uracil), disaccharides (maltose), alkaloids  
 542 (trigonelline), monosaccharides (glucose), benzamides (mytilitol),  
 543 carboxylic acid (glycolate), and sulfonic acid (hypotaurine) were higher in  
 544 the control condition. Conversely, the purines AMP and ADP, sulfonic acid  
 545 taurine, amino acids betaine and homarine, as well as FAs and conjugates  
 546 (2-aminobutyrate) were markers of *A. catenella* exposure.



547

548 **Figure 6.** Metabolomic analysis of the effect on the plasma of a 120h  
 549 exposure to *A. catenella*. (A) Contributions plot indicative of the  
 550 contribution of plasma metabolites identified in the OPLS-DA. (B) Score  
 551 plots following OPLS-DA. The plasma samples exposed to *A. catenella* and  
 552 the control are represented by pink and turquoise circles, respectively.  
 553 The model contained 32 buckets, 1 predictive and 1 orthogonal  
 554 components, and its descriptive and predictive performance were  $R^2Y =$   
 555  $0.92$  and  $Q^2 = 0.78$ .

556

## 557 4 **DISCUSSION**

558 In this work, we assessed some effects of a 120 h exposure of *M. edulis*  
559 to *A. catenella*. We determined a mean concentration in whole mussel soft  
560 tissues of 26 (23)  $\mu\text{g STX}/100\text{g}$  saxitoxin in the soft tissue, *i.e.*, below the  
561 threshold of 80  $\mu\text{g STXeq}/100\text{g}$  at which blue mussels are considered  
562 inedible (Bates et al., 2020). Nevertheless, significant effects were detected  
563 upon hemocyte activity, lipid composition, and metabolome, as well as  
564 mussel general metabolism as determined by the plasma metabolome.

### 565 **4.1 Immune cell responses to *A. catenella* exposure**

566 Our results showed that the percentage of live hemocytes in circulation  
567 was slightly higher following exposure to *A. catenella* as compared to the  
568 control group, despite possible lethal effects of toxins upon mussels, as  
569 reported by Bianchi et al. (2021). The moderate levels of toxins  
570 accumulated in mussels and short exposure time could explain this result.  
571 Hemocytes in exposed mussels were not going through the normal  
572 cellular death cycle because the production and use of hemocytes was  
573 necessary to respond to the toxic dinoflagellate by encapsulating and  
574 expelling them in the alimentary canal (Hegaret et al., 2007). Granulocytes  
575 are the most active phagocytic cells (Wikfors and Alix, 2014) and have a  
576 higher ability to produce ROS (de la Ballina et al., 2022). Our results showed  
577 that the granularity of the granulocytes was increased following toxic-  
578 algal treatment, which could be related to the internalization of algal  
579 toxins and detoxification through enzymatic activities. However, further  
580 analysis, such as measuring phagocyte activity of the hemocytes could

581 confirm this hypothesis. Active detoxification and elimination of toxin  
582 metabolites by diapedesis of hemocytes into the mussel gut (Galimany et  
583 al., 2008b) would leave fewer hemocytes cycling through apoptosis.

584 Conversely, the mortality of the agranulocytes was higher in the toxic  
585 treatment, suggesting that these cells are more vulnerable to microalgal  
586 toxins than the immuno-competent granular cells, as was observed for  
587 Pacific oyster *Crassostrea gigas* hemocytes exposed to saxitoxin (Abi-Khalil  
588 et al., 2017). Moreover, the ROS production by the agranulocytes from the  
589 STX-exposed mussels was higher, indicating a generalized stress  
590 response. It has been demonstrated that both hemocyte subpopulations  
591 contribute to the production of ROS, with the granulocytes being the most  
592 active cells (Andreyeva et al., 2019). Intracellular ROS increase in  
593 agranulocytes, as observed in our study, is seen in hypoxic conditions,  
594 consistent with the increased oxygen consumption rate previously  
595 recorded during exposure of mussels to *A. catenella* (Lavaud et al., 2021).  
596 Meanwhile, the production of ROS remained stable in granulocytes, as the  
597 intracellular ROS production is part of the detoxification, defense response  
598 (Bianchi et al., 2021). Thus, moderate levels of toxins may have an indirect  
599 effect upon the production of ROS in the agranulocytes, through the  
600 increase of oxygen consumption associated with stress.

#### 601 **4.2 Modification of hemocyte neutral lipid composition**

602 Exposing molluscs to harmful substances can affect the lipid  
603 composition of hemocytes (Leroux et al., 2022). *A. catenella* is no  
604 exception; our results showed that STX-exposed mussels responded with

605 a decrease in hemocyte neutral lipids (triacylglycerides (TAGs), ketones,  
606 sterols, acetone mobile polar lipids) in comparison to the control. A study  
607 of *M. galloprovincialis* hemocytes exposed to nanoplastics showed that  
608 TAGs were the most abundant class of lipids released into the culture  
609 medium, suggesting increased release of TAG-enriched vesicles (Leroux et  
610 al., 2022). Similarly, the lower concentration of neutral lipids in the  
611 hemocytes after exposure to *A. catenella* could be attributable to a  
612 preferential use in excretion vesicles containing the algal toxins or  
613 participation in ROS oxidative consumption. Some neutral lipids such as  
614 TAGs can also be used in the production of energy (Cantrell and Mohiuddin,  
615 2022). Indeed, immune stimulation is an energy-demanding process,  
616 therefore TAGs and phospholipids could be hydrolyzed by the hepatic  
617 lipases in the digestive gland to provide free FAs to maintain energy  
618 requirements, thereby limiting availability for the production of hemocytes  
619 (Qiu et al., 2020).

620 The FA composition was different between treatments only in the polar  
621 fraction. Two saturated FA (palmitic acid [16:0] and stearic acid [18:0]),  
622 one monounsaturated FA (MUFA) (eicosenoic acid [20:1n9]) and three  
623 polyunsaturated FAs (PUFA) (arachidonic acid [20:4n6], eicosapentaenoic  
624 acid [20:5n3], docohexaenoic acid [22:6n3]) were the major contributors  
625 to this difference (85%). More specifically, the two saturated FAs were  
626 more concentrated in the control, while the MUFAs and PUFAs were more  
627 concentrated in the STX-exposed hemocytes. This result suggest that  
628 hemocyte membrane lipids did not participate in the oxidation processes  
629 following increased ROS production induced by the *A. catenella* treatment,

630 which usually reduces by peroxidation the amount of MUFA and PUFAs  
631 (Winston et al., 1996).

#### 632 **4.3 Comparison of hemocyte and plasma metabolomics profiles**

633 Our analysis showed an 85% similarity in the metabolite composition of  
634 hemocyte extracts and plasma samples, but the plasma was richer and  
635 more concentrated in metabolites than the hemocyte extracts, as  
636 previously reported (Frizzo et al., 2021). Osmolytes (taurine, hypotaurine,  
637 betaine, Gly, Ala) had the highest signal intensity in both matrices,  
638 highlighting the importance of osmoconformity in mussel physiology, with  
639 amino acids being the most abundant compounds. The major difference  
640 between matrices was the presence of carboxylic acid salts (pyruvate,  
641 malate, malonate, galactarate), nucleotides (UMP, GMP), and tyramine in  
642 the hemocyte extracts, and the absence of glycolate, and 4-  
643 guanidinobutanoate (gamma amino acids). Pyruvate and malate are  
644 markers of energy metabolism in the cells, as pyruvate is the final product  
645 of glycolysis, and malate is involved in the Krebs cycle for the production  
646 of ATP. We cannot rule out that the glycolate circulating in the plasma  
647 could originate from algae in the mussel diet, because unicellular green  
648 algae can produce glycolate by photorespiration *via* oxygenation of  
649 ribulose-1,5-bisphosphate, usually during suboptimal growth periods at  
650 high temperatures (Taubert et al., 2019; Bruin et al., 1970). Only two  
651 molecules specific to molluscs were identified in the metabolomes:  
652 mytilitol (a cyclohexanol) and homarine (a pyridinecarboxylic acid) (Aru et  
653 al., 2020; Tikunov et al., 2010; Netherton and Gurin, 1982). Trigonelline, an



654 alkaloid product of the metabolism of niacin (vitamin B3), detected in  
655 vegetables and cereals, was putatively identified in both matrices. NMR  
656 signals similar to those for this metabolite have been detected in another  
657 study of mussels, but the presence of trigonelline in mussels has never  
658 been ascertained (Frizzo et al., 2021). This clearly illustrates the lack of  
659 knowledge of NMR signatures of metabolites specific to marine organisms  
660 and explains why almost 20% of the signals detected in the NMR spectra  
661 of the hemocytes and plasma could not be identified.

662 Nevertheless, this first attempt at establishing the effect of HAB on  
663 mussel hemocytes and general metabolomes showed changes in 47% and  
664 44% of the metabolites identified in the hemocytes and plasma,  
665 respectively.

#### 666 **4.3.1 *A. catenella* affects the energy metabolism of the hemocytes**

667 The effect of *A. catenella* upon the energy metabolism of the  
668 hemocytes was revealed by changes in several reporting molecules. The  
669 explicative and predictive OPLS-DA model based upon hemocyte data  
670 highlighted a higher level of carbohydrates (glucose, maltose) and ATP in  
671 the control. However, AMP and ADP were higher in STX-exposed mussels,  
672 indicating a modification of the energy balance in the hemocytes. The  
673 feeding of mussels exposed to the toxic dinoflagellate may also have been  
674 altered (discussed below), thus reducing the general production of ATP.  
675 Hemocytes may also use more energy to eliminate the algal toxins or to  
676 trigger ROS response (Cruz et al., 2007). The acetylcarnitine product of the  
677 reaction to produce the co-enzyme A (CoA) from acetyl-CoA and carnitine

678 was higher in the control hemocytes, which may be another indicator of a  
679 higher production of ATP in this group, as CoA is involved in the Krebs  
680 cycle.

681 UDP - a ribonucleoside diphosphate sometimes associated with glucose  
682 and involved in glycogenesis - was also higher in the control hemocytes.  
683 Indeed, before glucose can be stored as glycogen in granules (abundant in  
684 mussel granulocytes (Cajaraville and Pal, 1995)), the enzyme glycogen  
685 synthase combines UDP-glucose units to form a glycogen chain (Koyama et  
686 al., 2020; Gabbott and Whittle, 1986). The higher level of UDP/UDP-glucose in  
687 the control is consistent with a higher energetic status, as well as the  
688 higher content of carbohydrates, and may imply a higher ability to  
689 synthesize and store glycogen as energy storage. The related compounds  
690 uracil and UMP were also higher in the control group. Conversely, STX-  
691 exposed hemocytes may have lower glycogen storage and less energy  
692 since AMP and ADP (the products of ATP hydrolysis in cells) were higher.  
693 Glycogen could not be quantified as it was not extracted during sample  
694 preparation.

695 Two disruptors of mitochondrial functions, malonate and formate, were  
696 higher in the hemocytes of mussels exposed to *A. catenella*. Malonate  
697 can cause rapid mitochondrial potential collapse and ROS production that  
698 overwhelms the mitochondria's antioxidant capacity and leads to cell  
699 swelling (Fernandez-Gomez et al., 2005). Formate is a byproduct of acetate  
700 production and is responsible for the disruption of mitochondrial electron  
701 transport and energy production by inhibiting cytochrome oxidase

702 activity, the terminal electron acceptor of the electron transport chain.  
703 This mechanism can lead to cell death from depletion of ATP and  
704 increased production of cytotoxic ROS secondary to the blockade of the  
705 electron transport chain. Malonate and formate might be molecular  
706 precursors of the increased production of ROS by hemocyte mitochondria  
707 as a defense mechanism (Donaghy et al., 2012). They may also lead to  
708 hemocyte mortality when exposed to higher doses of STX, but not at such  
709 a low STX dose as achieved in the present study.

710 Bivalve cells rely upon free amino acids (FAA) to produce energy by  
711 oxidation or gluconeogenesis (Ponder et al., 2019). Our results do not,  
712 however, show a preference for this mode of energy production in the  
713 hemocytes. Indeed, some glucogenic amino acids were more present in  
714 the cytoplasm of the hemocytes exposed to *A. catenella* (Arg, Asp, Gly,  
715 Ile, Phe, sarcosine) and others (Ala, Ser, Trp) in the control group. The  
716 presence of FAAs also have another function: the regulation of isoosmotic  
717 cell volume, as will be discussed below.

#### 718 4.3.2 ***A. catenella* affects hemocyte osmolyte composition and** 719 **anti-oxidant profile**

720 To maintain normal cell and hemocyte-specific functions, organisms  
721 more primitive than crustaceans compensate for the salinity level in their  
722 environment by changing FAA concentrations. Aminopeptidase-I plays a  
723 critical role in creating this pool of amino acids that maintains the  
724 isoconformity in the cells, by breaking down proteins and polypeptides  
725 into FAAs at the lysosomal level (Hilbish and Koehn, 1987). In mussels, the

726 major osmolytes are Gly, Ala and its isomer  $\beta$ -Ala, taurine and their  
727 derivatives dimethylglycine, betaine (trimethylglycine) and hypotaurine.  
728 Homarine is derived from Gly and is specific to marine organisms. It is  
729 involved in methylation reactions to create betaine, and may also function  
730 as an osmolyte (May et al., 2017; Kube et al., 2007; Yancey, 2005), as does  
731 dimethylamine (Zhang et al., 2011).

732 Ala,  $\beta$ -Ala and taurine were higher in the hemocytes of the control  
733 group; whereas, Gly and dimethylglycine were lower as compared to the  
734 STX-exposed mussels. Other studies have reported that an increased  
735 concentration of  $\beta$ -Ala enhances carbohydrate metabolism in mussels  
736 (Wang et al., 2021), and is a taurine transport inhibitor (Jong et al., 2012). In  
737 addition, taurine has antioxidant properties, protecting the mitochondria  
738 against excessive superoxide generation (Jong et al., 2012). Thus, the lower  
739 level of the anti-oxidant taurine in the hemocytes following the toxic  
740 treatment could help maintain production of ROS by mitochondria as part  
741 of the immune response (Winston et al., 1996).

742 Interestingly, only Ala varied in the same way as OPLS-DA adjusted to  
743 the plasma metabolites. Hypotaurine, Ala and dimethylglycine were  
744 higher in the plasma of the controls, but betaine, taurine, and homarine  
745 were higher in the plasma following toxic treatment. The higher contents  
746 of betaine and taurine – two antioxidants – in the exposed mussels may  
747 have a protective effect against ROS (Liang et al., 2020; Zhang et al., 2016).  
748 Mussels exposed to toxins tended to produce more ROS, which induced an  
749 antioxidant and detoxifying response involving enzymes such as

750 superoxide dismutase or glutathione-S-transferase, but also molecules  
751 such as glutathione (Liu et al., 2020) or betaine and taurine.

#### 752 **4.3.3 *A. catenella* seems to affect food intake**

753 The OPLS-DA model showed lower carbohydrates (maltose, glucose),  
754 but also UDP/UDP-glucose and uracil (see above) circulating in the plasma  
755 of mussels exposed to the toxic dinoflagellate, suggesting that mussels  
756 may stop or reduce feeding as reported in juvenile oysters (Cassis, 2005).  
757 The behavioral response of oysters when exposed to toxigenic  
758 *Alexandrium* spp., which also produce STX, is complete closure and  
759 feeding cessation. In *M. edulis* mussels, the response is different. At  
760 intermediary algal densities, similar to that archived in our experimental  
761 conditions, increased valve opening could be explained by a paralysis of  
762 the adductor muscle, potentially interfering with the control of the  
763 filtration process (Durier et al., 2022). Glycolate – a molecule that could  
764 originate from the algae in the diet – as well as all the amino acids present  
765 in the model based upon the plasma [Arg, Asp, Gln, Glu, Phe, Ser, Trp, Tyr,  
766 ornithine (a precursor of Arg), and 2-aminobutyrate (Ile biosynthesis)],  
767 were also in lower levels in mussels exposed to the toxic treatment, which  
768 could be another indicator of lower feed intake. Moreover, the higher level  
769 of ATP-hydrolysis products (ADP, AMP) in the plasma may be indicative of  
770 lower energy following feeding cessation exacerbated by the higher need  
771 for energy to reject the toxic dinoflagellates and eliminate toxins that  
772 made it inside the organism.

773 5 **CONCLUSION**

774 This work intended to study the effect of a HAB upon blue mussel  
775 immune response. A 120 h exposure of blue mussels to *A. catenella* led to  
776 moderate STX contamination of the tissues, with an average  
777 concentration of 26 (23)  $\mu\text{g}$  STX/100 g of mussel soft tissues. At this sub-  
778 lethal toxin concentration (Bricelj et al., 2005), several effects upon  
779 hemocyte activity were detected. The aggregated changes are consistent  
780 with activation of defense mechanisms in granular hemocytes and a  
781 stress response in agranular cells, both consuming energy and changing  
782 the overall metabolic status of the mussels.

783 The implementation of  $^1\text{H}$  NMR-based metabolomics as a high-  
784 throughput profiling and classification tool opens new perspectives to  
785 understand the effects of HAB upon mussel general and immune  
786 metabolisms. This study offers a new approach to decipher biochemical  
787 pathways in mussels, involving hemocyte activity measurement, lipid  
788 composition determination, and the first NMR-detected metabolomic  
789 investigation of hemocytes and their plasma.

790

791 **DECLARATION OF COMPETING INTEREST**

792 The authors have no known competing financial interests or personal  
793 relationships that could have appeared to influence the work reported in  
794 this paper.

795

**796 Author contributions**

797 S.B. drafted the manuscript, performed the NMR-based metabolomics,  
798 chemometrics, and biological integration. O.G. carried out the index  
799 measurements and lipid composition analysis under the supervision of  
800 R.T. as well as the cytometry analyzes under the supervision of G.H.W.  
801 B.G. established the SXT dosage method and performed the analyses.  
802 A.A.A. and D.E.W. contributed to the development of the NMR  
803 experiments applied to mussel hemocytes. R.T. and I.M. designed and  
804 supervised the study. S.B., A.A.A., D.E.W, G.H.W., R.T., and I. M.  
805 contributed to write the manuscript. All authors have approved the final  
806 article.

**807 Acknowledgements**

808 This project was supported by Environment and Climate Change Canada  
809 (FDE-CA-2017i002 to R.T.), the Natural Sciences and Engineering  
810 Research Council (NSERC) of Canada (grant RGPIN-2018-06200 to I.M.)  
811 and the Ressources Aquatiques Québec research network (Fonds de  
812 Recherche du Québec - Nature et Technologies, no. 2014-RS-171172).  
813 Fisheries and Oceans Canada provided in-kind assistance motivated by  
814 the Galway Statement on Atlantic Ocean Cooperation. The authors wish to  
815 thank Nathalie Gauthier and Jean-Bruno Nadalini for technical support and  
816 Tiago Hori from Atlantic Aqua Farms to supply mussels. Pr. Lekha Sleno as  
817 well as Leanne Ohlund (UQAM) are acknowledged for laboratory access  
818 and technical help support. All authors are members of Ressources  
819 Aquatiques Québec.

820 **Funding**

821 This project was supported by Environment and Climate Change Canada  
 822 (FDE-CA-2017i002 to R.T.), the Natural Sciences and Engineering  
 823 Research Council (NSERC) of Canada (grant RGPIN-2018-06200 to I.M.)  
 824 and the Ressources Aquatiques Québec research network (Fonds de  
 825 Recherche du Québec – Nature et Technologies, no. 2014-RS-171172).

826 **References**

- 827 ~~Abi-Khalil~~, C., Finkelstein, D.S., Conejero, G., du Bois, J., Destoumieux-Garzon, D.,  
 828 Rolland, J.L., 2017. The paralytic shellfish toxin, saxitoxin, enters the cytoplasm  
 829 and induces apoptosis of oyster immune cells through a caspase-dependent  
 830 pathway. *Aquatic Toxicology* 190, 133-141.  
 831 <https://doi.org/https://doi.org/10.1016/j.aquatox.2017.07.001>
- 832 ~~Andreyeva~~, A.Y., Efremova, E.S., Kukhareva, T.A., 2019. Morphological and functional  
 833 characterization of hemocytes in cultivated mussel (*Mytilus galloprovincialis*) and  
 834 effect of hypoxia on hemocyte parameters. *Fish Shellfish Immunol* 89, 361-367.  
 835 <https://doi.org/https://doi.org/10.1016/j.fsi.2019.04.017>
- 836 ~~Ar~~, V., Motawie, M.S., Khakimov, B., Sørensen, K.M., Møller, B.L., Engelsen, S.B.,  
 837 2020. First-principles identification of C-methyl-scylo-inositol (mytilitol) - A new  
 838 species-specific metabolite indicator of geographic origin for marine bivalve  
 839 molluscs (*Mytilus* and *Ruditapes* spp.). *Food Chem* 328, 126959.  
 840 <https://doi.org/10.1016/j.foodchem.2020.126959>
- 841 ~~Bates~~, S.S., Beach, D.G., Comeau, L.A., Haigh, N., Lewis, N.I., Locke, A., Martin, J.L.,  
 842 Mccarron, P., Mckenzie, C.H., Michel, C., Miles, C.O., Poulin, M., Quilliam, M.A.,  
 843 Rourke, W.A., Scarratt, M.G., Starr, M., Wells, T., 2020. Marine harmful algal  
 844 blooms and phycotoxins of concern to Canada Canadian Technical Report of  
 845 Fisheries and Aquatic Sciences 3384. *Can. Tech. Rep. Fish. Aquat. Sci.* 3384.
- 846 ~~Bayona~~, L.M., de Voogd, N.J., Choi, Y.H., 2022. Metabolomics on the study of marine  
 847 organisms. *Metabolomics* 18, 17. <https://doi.org/10.1007/s11306-022-01874-y>
- 848 ~~Beauclercq~~, S., Mignon-Grasteau, S., Petit, A., Berger, Q., Lefèvre, A., Métayer-  
 849 Coustard, S., Tesseraud, S., Emond, P., Berri, C., Le Bihan-Duval, E., 2022. A  
 850 Divergent Selection on Breast Meat Ultimate pH, a Key Factor for Chicken Meat  
 851 Quality, is Associated With Different Circulating Lipid Profiles. *Front Physiol* 13.  
 852 <https://doi.org/10.3389/fphys.2022.935868>
- 853 ~~Bianchi~~, V.A., Bickmeyer, U., Tillmann, U., Krock, B., Müller, A., Abele, D., 2021. In  
 854 Vitro Effects of Paralytic Shellfish Toxins and Lytic Extracellular Compounds  
 855 Produced by Alexandrium Strains on Hemocyte Integrity and Function in *Mytilus*  
 856 *edulis*. *Toxins (Basel)* 13. <https://doi.org/10.3390/toxins13080544>
- 857 ~~Bianchi~~, V.A., Langeloh, H., Tillmann, U., Krock, B., Müller, A., Bickmeyer, U., Abele,  
 858 D., 2019. Separate and combined effects of neurotoxic and lytic compounds of  
 859 Alexandrium strains on *Mytilus edulis* feeding activity and hemocyte function.  
 860 *Fish Shellfish Immunol* 84, 414-422.  
 861 <https://doi.org/https://doi.org/10.1016/j.fsi.2018.10.024>



- 862 Masco, D., Levasseur, M., Bonneau, E., Gelinas, R., Packard, T.T., 2003. Patterns of  
863 paralytic shellfish toxicity in the St. Lawrence region in relationship with the  
864 abundance and distribution of *Alexandrium tamarense*. *Sci Mar* 67, 261–278.
- 865 Boivin-Rioux, A., Starr, M., Chassé, J., Scarratt, M., Perrie, W., Long, Z., 2021.  
866 Predicting the Effects of Climate Change on the Occurrence of the Toxic  
867 Dinoflagellate *Alexandrium catenella* Along Canada's East Coast. *Front Mar Sci*.
- 868 Bricej, V.M., Connell, L., Konoki, K., MacQuarrie, S.P., Scheuer, T., Catterall, W.A.,  
869 Trainer, V.L., 2005. Sodium channel mutation leading to saxitoxin resistance in  
870 clams increases risk of PSP. *Nature* 434, 763–767.  
871 <https://doi.org/10.1038/nature03415>
- 872 Bruin, W.J., Nelson, E.B., Tolbert, N.E., 1970. Glycolate pathway in green algae. *Plant*  
873 *Physiol* 46, 386–391. <https://doi.org/10.1104/pp.46.3.386>
- 874 Caraville, M.P., Pal, S.G., 1995. Morphofunctional study of the haemocytes of the  
875 bivalve mollusc *Mytilus galloprovincialis* with emphasis on the endolysosomal  
876 compartment. *Cell Struct Funct* 20, 355–367. <https://doi.org/10.1247/CSF.20.355>
- 877 Campos, A., Apraiz, I., da Fonseca, R.R., Cristobal, S., 2015. Shotgun analysis of the  
878 marine mussel *Mytilus edulis* hemolymph proteome and mapping the innate  
879 immunity elements. *Proteomics* 15, 4021–4029.  
880 <https://doi.org/https://doi.org/10.1002/pmic.201500118>
- 881 Cantrell, C.B., Mohiuddin, S.S., 2022. Biochemistry, Ketone Metabolism, in: *StatPearls*.  
882 StatPearls Publishing LLC., Treasure Island (FL).
- 883 Cassis, D., 2005. The effect of harmful algae on the summer mortality of juvenile  
884 pacific oysters (*Crassostrea gigas*). The University of British Columbia,  
885 Vancouver.
- 886 Cheng 1, T.C., 1996. Haemocytes: forms and functions. In: Kennedy, V., Newell, R.,  
887 Eble, A. (Eds.), *The Eastern Oyster Crassostrea Virginica*. College Park: Maryland  
888 Sea Grant, pp. 299–333.
- 889 Comeau, L.A., Babarro, J.M.F., Riobó, P., Scarratt, M., Starr, M., Tremblay, R., 2019.  
890 PSP-producing dinoflagellate *Alexandrium minutum* induces valve microclosures  
891 in the mussel *Mytilus galloprovincialis*. *Aquaculture* 500, 407–413.  
892 <https://doi.org/https://doi.org/10.1016/j.aquaculture.2018.10.025>
- 893 Cruz, C.M., Rinna, A., Forman, H.J., Ventura, A.L.M., Persechini, P.M., Ojcius, D.M.,  
894 2007. ATP Activates a Reactive Oxygen Species-dependent Oxidative Stress  
895 Response and Secretion of Proinflammatory Cytokines in Macrophages. *Journal of*  
896 *Biological Chemistry* 282, 2871–2879. <https://doi.org/10.1074/JBC.M608083200>
- 897 Cusick, K.D., Sayler, G.S., 2013. An Overview on the Marine Neurotoxin, Saxitoxin:  
898 Genetics, Molecular Targets, Methods of Detection and Ecological Functions. *Mar*  
899 *Drugs* 11, 991–1018.
- 900 de la Ballina, N.R., Maresca, F., Cao, A., Villalba, A., 2022. Bivalve Haemocyte  
901 Subpopulations: A Review. *Front Immunol* 13, 826255.  
902 <https://doi.org/10.3389/fimmu.2022.826255>

- 903 Delaporte, M., Soudant, P., Moal, J., Giudicelli, E., Lambert, C., Segueineau, C., Samain,  
904 J.F., 2006. Impact of 20 : 4n-6 supplementation on the fatty acid composition and  
905 hemocyte parameters of the Pacific oyster *Crassostrea gigas*. *Lipids* 41, 567-576.
- 906 Digilio, G., Sforzini, S., Cassino, C., Robotti, E., Oliveri, C., Marengo, E., Musso, D.,  
907 Osella, D., Viarengo, A., 2016. Haemolymph from *Mytilus galloprovincialis*:  
908 Response to copper and temperature challenges studied by <sup>1</sup>H-NMR  
909 metabonomics. *Comparative Biochemistry and Physiology Part C: Toxicology &*  
910 *Pharmacology* 183-184, 61-71. <https://doi.org/10.1016/j.CBPC.2016.02.003>
- 911 Donaghy, L., Kraffe, E., Goïc, N., Lambert, C., Volety, A.K., Soudant, P., 2012. Reactive  
912 oxygen species in unstimulated hemocytes of the Pacific oyster *Crassostrea gigas*:  
913 a mitochondrial involvement. *PLoS One* 7.  
914 <https://doi.org/10.1371/journal.pone.0046594>
- 915 Durier, G., Nadalini, J.B., Comeau, L.A., Starr, M., Michaud, S., Tran, D., St-Louis, R.,  
916 Babarro, J.M.F., Clements, J.C., Tremblay, R., 2022. Use of valvometry as an alert  
917 tool to signal the presence of toxic algae *Alexandrium catenella* by *Mytilus*  
918 *edulis*. *Front Mar Sci* 9, 1930.  
919 <https://doi.org/10.3389/FMARS.2022.987872/BIBTEX>
- 920 FAO, 2020. The State of World Fisheries and Aquaculture 2020. Sustainability in  
921 action. Rome. <https://doi.org/https://doi.org/10.4060/ca9229en>
- 922 Fernandez-Gomez, F.J., Galindo, M.F., Gómez-Lázaro, M., Yuste, V.J., Comella, J.X.,  
923 Aguirre, N., Jordán, J., 2005. Malonate induces cell death via mitochondrial  
924 potential collapse and delayed swelling through an ROS-dependent pathway. *Br J*  
925 *Pharmacol* 144, 528. <https://doi.org/10.1038/SJ.BJP.0706069>
- 926 Frizzo, R., Bortoletto, E., Riello, T., Leanza, L., Schievano, E., Venier, P., Mammi, S.,  
927 2021. NMR Metabolite Profiles of the Bivalve Mollusc *Mytilus galloprovincialis*  
928 Before and After Immune Stimulation With *Vibrio splendidus*. *Front Mol Biosci* 8,  
929 731. <https://doi.org/10.3389/FMOLB.2021.686770/BIBTEX>
- 930 Gabbott, P.A., Whittle, M.A., 1986. Glycogen synthetase in the sea mussel *Mytilus*  
931 *edulis* L.—II. Seasonal changes in glycogen content and glycogen synthetase  
932 activity in the mantle tissue. *Comparative Biochemistry and Physiology Part B:*  
933 *Comparative Biochemistry* 83, 197-207. <https://doi.org/10.1016/0305->  
934 [0491\(86\)90353-6](https://doi.org/10.1016/0305-0491(86)90353-6)
- 935 Galimany, E., Sunila, I., Hegaret, H., Ramon, M., Wikfors, G.H., 2008a. Pathology and  
936 immune response of the blue mussel (*Mytilus edulis* L.) after an exposure to the  
937 harmful dinoflagellate *Prorocentrum minimum*. *Harmful Algae* 7, 630-638.  
938 <https://doi.org/10.1016/j.hal.2008.01.001>
- 939 Galimany, E., Sunila, I., Hégaret, H., Ramón, M., Wikfors, G.H., 2008b. Experimental  
940 exposure of the blue mussel (*Mytilus edulis*, L.) to the toxic dinoflagellate  
941 *Alexandrium fundyense*: Histopathology, immune responses, and recovery.  
942 *Harmful Algae* 7, 702-711.  
943 <https://doi.org/http://dx.doi.org/10.1016/j.hal.2008.02.006>
- 944 Gosling, E., 2008. Bivalve molluscs: biology, ecology and culture. John Wiley & Sons.

- 945 Hégaret, H., Wikfors, G.H., Shumway, S.E., 2007. Diverse feeding responses of five  
946 species of bivalve mollusc when exposed to three species of harmful algae. J.  
947 Shellfish Res. 26, 549–559.
- 948 Hégaret, H., Wikfors, G.H., Soudant, P., 2003. Flow-cytometric analysis of haemocytes  
949 from eastern oysters, *Crassostrea virginica*, subjected to a sudden temperature  
950 elevation: I. Haemocyte types and morphology. J. Exp. Mar. Biol. Ecol. 293, 237–  
951 248.
- 952 Ilbish, T.J., Koehn, R.K., 1987. The Adaptive Importance of Genetic Variation. Am Sci  
953 75, 134–141.
- 954 Jacob, D., Deborde, C., Lefebvre, M., Maucourt, M., Moing, A., 2017. NMRProcFlow: a  
955 graphical and interactive tool dedicated to 1D spectra processing for NMR-based  
956 metabolomics. Metabolomics 13, 36. <https://doi.org/10.1007/s11306-017-1178-y>
- 957 John, U., Litaker, W., Montresor, M., Murray, S., Brosnahan, M.L., Anderson, D.M.,  
958 2014. (2302) Proposal to reject the name *Gonyaulax catenella* (Alexandrium  
959 catenella) (Dinophyceae). Taxon 63, 932. <https://doi.org/10.12705/634.21>
- 960 Ong, C.J., Azuma, J., Schaffer, S., 2012. Mechanism underlying the antioxidant  
961 activity of taurine: prevention of mitochondrial oxidant production. Amino Acids  
962 42, 2223–2232. <https://doi.org/10.1007/s00726-011-0962-7>
- 963 Oyama, M., Furukawa, F., Koga, Y., Funayama, S., Furukawa, S., Baba, O., Lin, C.C.,  
964 Hwang, P.P., Moriyama, S., Okumura, S.I., 2020. Gluconeogenesis and glycogen  
965 metabolism during development of Pacific abalone, *Haliotis discus hannai*. Am J  
966 Physiol Regul Integr Comp Physiol 318, R619–R633.  
967 <https://doi.org/10.1152/AJPREGU.00211.2019/ASSET/IMAGES/LARGE/ZH60032098>  
968 310008.JPEG
- 969 Ube, S., Sokolowski, A., Jansen, J.M., Schiedek, D., 2007. Seasonal variability of free  
970 amino acids in two marine bivalves, *Macoma balthica* and *Mytilus* spp., in  
971 relation to environmental and physiological factors. Comp Biochem Physiol A Mol  
972 Integr Physiol 147, 1015–1027. <https://doi.org/10.1016/j.cbpa.2007.03.012>
- 973 Lassudrie, M., Hégaret, H., Wikfors, G.H., da Silva, P.M., 2020. Effects of marine  
974 harmful algal blooms on bivalve cellular immunity and infectious diseases: A  
975 review. Dev Comp Immunol 108, 103660.
- 976 Lavaud, R., Durier, G., Nadalini, J.-B., Filgueira, R., Comeau, L.A., Babarro, J.M.F.,  
977 Michaud, S., Scarratt, M., Tremblay, R., 2021. Effects of the toxic dinoflagellate  
978 *Alexandrium catenella* on the behaviour and physiology of the blue mussel  
979 *Mytilus edulis*. Harmful Algae 108, 102097.  
980 <https://doi.org/https://doi.org/10.1016/j.hal.2021.102097>
- 981 Grand, F., Kraffe, E., Marty, Y., Donaghy, L., Soudant, P., 2011. Membrane  
982 phospholipids compositions of hemocytes in the Pacific oyster *Crassostrea gigas*  
983 and the Manila clam *Ruditapes philippinarum*. Comp. Biochem. Physiol. 159A,  
984 383–391.
- 985 Grand, F., Soudant, P., Marty, Y., le Goïc, N., Kraffe, E., 2013. Altered membrane  
986 lipid composition and functional parameters of circulating cells in cockles  
987 (*Cerastoderma edule*) affected by disseminated neoplasia. Chem Phys Lipids  
988 167–168, 9–20.

- 988 Grand, F., Soudant, P., Siah, A., Tremblay, R., Marty, Y., Kraffe, E., 2014.  
 990 Disseminated neoplasia in the soft-shell clam *Mya arenaria*: Membrane lipid  
 991 composition and functional parameters of circulating cells. *Lipids* 49, 807–818.
- 992 Leroux, N., Hosseinzadeh, M., Katsumiti, A., Porte, C., Cajaraville, M.P., 2022.  
 993 Lipidomic analysis of mussel hemocytes exposed to polystyrene nanoplastics.  
 994 *Environ Res* 214, 113763.  
 995 <https://doi.org/https://doi.org/10.1016/j.envres.2022.113763>
- 996 Tang, R., Shao, X., Shi, Y., Jiang, L., Han, G., 2020. Antioxidant defenses and  
 997 metabolic responses of blue mussels (*Mytilus edulis*) exposed to various  
 998 concentrations of erythromycin. *Science of The Total Environment* 698, 134221.  
 999 <https://doi.org/10.1016/J.SCITOTENV.2019.134221>
- 1000 Lu, Y., Li, L., Zheng, L., Fu, P., Wang, Y., Nguyen, H., Shen, X., Sui, Y., 2020.  
 1001 Antioxidant responses of triangle sail mussel *Hyriopsis cumingii* exposed to  
 1002 harmful algae *Microcystis aeruginosa* and high pH. *Chemosphere* 243, 125241.  
 1003 <https://doi.org/10.1016/J.CHEMOSPHERE.2019.125241>
- 1004 Madji Hounoum, B., Blasco, H., Nadal-Desbarats, L., Diémé, B., Montigny, F., Andres,  
 1005 C.R., Emond, P., Mavel, S., 2015. Analytical methodology for metabolomics study  
 1006 of adherent mammalian cells using NMR, GC-MS and LC-HRMS. *Anal Bioanal*  
 1007 *Chem* 407, 8861–8872. <https://doi.org/10.1007/s00216-015-9047-x>
- 1008 May, M.A., Bishop, K.D., Rawson, P.D., 2017. NMR Profiling of Metabolites in Larval  
 1009 and Juvenile Blue Mussels (*Mytilus edulis*) under Ambient and Low Salinity  
 1010 Conditions. *Metabolites* 7. <https://doi.org/10.3390/METABO7030033>
- 1011 Netherton, J.C., Gurin, S., 1982. Biosynthesis and physiological role of homarine in  
 1012 marine shrimp. *Journal of Biological Chemistry* 257, 11971–11975.  
 1013 [https://doi.org/10.1016/s0021-9258\(18\)33662-7](https://doi.org/10.1016/s0021-9258(18)33662-7)
- 1014 Nguyen, T. v, Alfaro, A.C., 2020. Applications of omics to investigate responses of  
 1015 bivalve haemocytes to pathogen infections and environmental stress.  
 1016 *Aquaculture* 518, 734488.  
 1017 <https://doi.org/https://doi.org/10.1016/j.aquaculture.2019.734488>
- 1018 Nielsen, L.T., Hansen, P.J., Krock, B., Vismann, B., 2016. Accumulation, transformation  
 1019 and breakdown of DSP toxins from the toxic dinoflagellate *Dinophysis acuta* in  
 1020 blue mussels, *Mytilus edulis*. *Toxicon* 117, 84–93.  
 1021 <https://doi.org/10.1016/J.TOXICON.2016.03.021>
- 1022 Parrish, C., 1987. Separation of aquatic lipid classes by chromarod thin-layer  
 1023 chromatography with measurement by Iatroscan Flame Ionization detection.  
 1024 *Can. J. Fish. Aquat. Sci.* 44, 722–731.
- 1025 Parrish, C.C., 1999. Determination of total lipid, lipid classes, and fatty acids in  
 1026 aquatic samples, in: Arts, M.T., Wainman, B.C. (Eds.), *Lipids in Freshwater*  
 1027 *Ecosystems*. Springer-Verlag, New York., pp. 4–20.
- 1028 Ponder, W.F., Lindberg, D.R., Ponder, J.M., 2019. Overview of Molluscan Physiology  
 1029 and Genomics, in: *Biology and Evolution of the Mollusca*. Taylor & Francis, Boca  
 1030 Raton.

- 1031 Pousse, É., Flye-Sainte-Marie, J., Alunno-Bruscia, M., Hégaret, H., Rannou, É.,  
 1032 Pecquerie, L., Marques, G.M., Thomas, Y., Castrec, J., Fabioux, C., Long, M.,  
 1033 Lassudrie, M., Hermabessiere, L., Amzil, Z., Soudant, P., Jean, F., 2019. Modelling  
 1034 paralytic shellfish toxins (PST) accumulation in *Crassostrea gigas* by using  
 1035 Dynamic Energy Budgets (DEB). *J Sea Res* 143, 152-164.  
 1036 <https://doi.org/https://doi.org/10.1016/j.seares.2018.09.002>
- 1037 Qiu, J., Ji, Y., Fang, Y., Zhao, M., Wang, S., Ai, Q., Li, A., 2020. Response of fatty acids  
 1038 and lipid metabolism enzymes during accumulation, depuration and  
 1039 esterification of diarrhetic shellfish toxins in mussels (*Mytilus galloprovincialis*).  
 1040 *Ecotoxicol Environ Saf* 206, 111223.  
 1041 <https://doi.org/https://doi.org/10.1016/j.ecoenv.2020.111223>
- 1042 Soudant, P., Paillard, C., Choquet, G., Lambert, C., Reid, H.I., Marhic, A., Donaghy, L.,  
 1043 Birkbeck, T.H., 2004. Impact of season and rearing site on the physiological and  
 1044 immunological parameters of the Manila clam *Venerupis* (=Tapes, =Ruditapes)  
 1045 philippinarum. *Aquaculture* 229, 401-418.
- 1046 Starr, M., Lair, S., Michaud, S., Scarratt, M., Quilliam, M., Lefavre, D., Robert, M.,  
 1047 Wotherspoon, A., Michaud, R., Ménard, N., Sauv e, G., Lessard, S., B eland, P.,  
 1048 Measures, L., 2017. Multispecies mass mortality of marine fauna linked to a toxic  
 1049 dinoflagellate bloom. *PLoS One* 12, e0176299.  
 1050 <https://doi.org/10.1371/journal.pone.0176299>
- 1051 Statistics-Canada, 2019. Statistique Canada. (2019). Production d'aquaculture en  
 1052 quantit e et en valeurs. <https://www.dfo-mpo.gc.ca/stats/aqua/aqua19-fra.htm>.
- 1053 Saubert, A., Jakob, T., Wilhelm, C., 2019. Glycolate from microalgae: an efficient  
 1054 carbon source for biotechnological applications. *Plant Biotechnol J* 17, 1538-  
 1055 1546. <https://doi.org/https://doi.org/10.1111/pbi.13078>
- 1056 Sukunov, A.P., Johnson, C.B., Lee, H., Stoskopf, M.K., Macdonald, J.M., 2010.  
 1057 Metabolomic investigations of American oysters using H-NMR spectroscopy. *Mar*  
 1058 *Drugs* 8, 2578-2596. <https://doi.org/10.3390/md8102578>
- 1059 Fran, D., Haberkorn, H., Soudant, P., Ciret, P., Massabuau, J.-C., 2010. Behavioral  
 1060 responses of *Crassostrea gigas* exposed to the harmful algae *Alexandrium*  
 1061 *minutum*. *Aquaculture* 298, 338-345.
- 1062 Tremblay, R., Landry, T., 2016. The implication of metabolic performance of *Mytilus*  
 1063 *edulis*, *Mytilus trossulus*, and hybrids for mussel aquaculture in eastern canadian  
 1064 waters. *Journal of Marine Biology and Aquaculture* 2, 1-7.
- 1065 Currens, J.F., 2003. Mitochondrial formation of reactive oxygen species. *J Physiol* 552,  
 1066 335-344. <https://doi.org/https://doi.org/10.1111/j.1469-7793.2003.00335.x>
- 1067 Wang, C. yue, Yan, X. jun, He, J. yu, Buttino, I., Pan, C., Fan, M. hua, Guo, B. ying,  
 1068 Zhang, X. lin, Liao, Z., 2021. Responses to  $\beta$ -alanine and carnosine  
 1069 supplementation of mussel *Mytilus coruscus* as revealed by UPLC-MS/MS based  
 1070 untargeted metabolomics. *Aquac Rep* 20, 100730.  
 1071 <https://doi.org/10.1016/j.AQREP.2021.100730>
- 1072 Wang, J., Salata, J.J., Bennett, P.B., 2003. Saxitoxin is a gating modifier of HERG K+  
 1073 channels. *J Gen Physiol* 121, 583-598. <https://doi.org/10.1085/jgp.200308812>

- 1074 Wikfors, G.H., Alix, J.H., 2014. Granular hemocytes are phagocytic, but agranular  
1075 hemocytes are not, in the Eastern Oyster *Crassostrea virginica*. *Invertebrate*  
1076 *Immunity* 1. <https://doi.org/10.2478/INVIM-2014-0001>
- 1077 Winston, G.W., Moore, M.N., Kirchin, M.A., Soverchia, C., 1996. Production of reactive  
1078 oxygen species by Hemocytes from the marine mussel, *Mytilus edulis*: Lysosomal  
1079 localization and effect of xenobiotics. *Comp Biochem Physiol C Pharmacol Toxicol*  
1080 *Endocrinol* 113, 221–229. [https://doi.org/10.1016/0742-8413\(95\)02091-8](https://doi.org/10.1016/0742-8413(95)02091-8)
- 1081 Wishart, D.S., Guo, A., Oler, E., Wang, F., Anjum, A., Peters, H., Dizon, R., Sayeeda, Z.,  
1082 Tian, S., Lee, B.L., Berjanskii, M., Mah, R., Yamamoto, M., Jovel, J., Torres-Calzada,  
1083 C., Hiebert-Giesbrecht, M., Lui, V.W., Varshavi, D., Varshavi, D., Allen, D., Arndt,  
1084 D., Khetarpal, N., Sivakumaran, A., Harford, K., Sanford, S., Yee, K., Cao, X.,  
1085 Budinski, Z., Liigand, J., Zhang, L., Zheng, J., Mandal, R., Karu, N., Dambrova, M.,  
1086 Schiöth, H.B., Greiner, R., Gautam, V., 2022. HMDB 5.0: the Human Metabolome  
1087 Database for 2022. *Nucleic Acids Res* 50, D622-d631.  
1088 <https://doi.org/10.1093/nar/gkab1062>
- 1089 Pancey, P.H., 2005. Organic osmolytes as compatible, metabolic and counteracting  
1090 cytoprotectants in high osmolarity and other stresses. *Journal of Experimental*  
1091 *Biology* 208, 2819–2830. <https://doi.org/10.1242/JEB.01730>
- 1092 Dung, T., Alfaro, A.C., 2018. Metabolomic strategies for aquaculture research: a  
1093 primer. *Rev Aquac* 10, 26–56. <https://doi.org/https://doi.org/10.1111/raq.12146>
- 1094 Zacharias, H.U., Altenbuchinger, M., Gronwald, W., 2018. Statistical Analysis of NMR  
1095 Metabolic Fingerprints: Established Methods and Recent Advances. *Metabolites*  
1096 8. <https://doi.org/10.3390/metabo8030047>
- 1097 Zhang, L., Liu, X., You, L., Zhou, D., Wu, H., Li, L., Zhao, J., Feng, J., Yu, J., 2011.  
1098 Metabolic responses in gills of Manila clam *Ruditapes philippinarum* exposed to  
1099 copper using NMR-based metabolomics. *Mar Environ Res* 72, 33–39.  
1100 <https://doi.org/10.1016/J.MARENRES.2011.04.002>
- 1101 Zhang, M., Zhang, H., Li, H., Lai, F., Li, X., Tang, Y., Min, T., Wu, H., 2016. Antioxidant  
1102 Mechanism of Betaine without Free Radical Scavenging Ability. *J Agric Food*  
1103 *Chem* 64, 7921–7930.  
1104 <https://doi.org/10.1021/ACS.JAFC.6B03592/ASSET/IMAGES/LARGE/JF-2016->  
1105 [03592Z\\_0007.JPEG](https://doi.org/10.1021/ACS.JAFC.6B03592/ASSET/IMAGES/LARGE/JF-2016-03592Z_0007.JPEG)
- 1106